FAR INFRA-RED SPECTROSCOPIC STUDIES

OF

GASEOUS AND LIQUID MOLECULAR SYSTEMS

A thesis submitted to the

UNIVERSITY OF WALES

for the degree of

PHILOSOPHIAE DOCTOR

by

Myron Wyn Evans, B.Sc. (Wales)

DECLARATION

The experimental work described in this thesis was carried out by me either at the Edward Davies Chemical Laboratories, University College of Wales, Aberystwyth, or else at the National Physical Laboratory, Teddington, Middlesex.

In the cases (Chapters 6 and 7) where the candidate is a part author, the work carried out solely by the candidate consists of:

(i) all the experimental;

(ii) the model calculation, computation, and curve fitting in Chapters 6 and 7.

I declare that this work has not already been accepted in substance for any degree, and is not being concurrently submitted in candidature for any degree.

Signed: M. W. Evans.....

Supervisor: Marcel Davies

Date: 9th July, 1974.

Acknowledgements

I wish to record my indebtedness to Professor Mansel Davies for many original ideas, and for getting me started on varied and fascinating investigations during the last three years or so.

There were also words of advice from Drs. Alun Price and Graham Williams and Ian Larkin which did not go unheeded. I also thank Dr. Arnold Baise for teaching me the use of the apparatus at Aberystwyth, and Drs. Fleming and Nichols for a similar favour at the National Physical Laboratory. I thank Drs. Graham Davies and Jim Kettle for rounding off my education in the experimental side, and Mr. Peter Deft for stimulating criticism of the work on MBBA.

These researches would have been much more difficult to carry out without the skills of John Poley, Harold Jolley, and Bob Meredith in the Mechanical Workshop, and I wish to thank all the members of the technical staff at Aberystwyth for their help, especially over the last three years. I also thank U.C.W., Aberystwyth Computer Unit for their efficiency.

I thank the University of Wales for the award of a Dr. Samuel Williams Studentship. Last, but not least, Mrs. D. Jones is thanked for typing this thesis.

Summary

The origins of compressed gaseous and liquid phase absorptions in the 6 - 200 cm^{-1} region of dipolar and non-dipolar molecules have been investigated. The gaseous data have been treated in terms of a bimolecular collision model, assuming absorptions in excess of those due to rotations of permanent dipoles to arise from a dipole induced in one molecule by the field of another. The apparent point quadrupole moment of the inducing field has been evaluated for the non-dipolar species cyanogen, whose absorption is entirely collision induced. This value is much reduced in the liquid phase, reflecting the reduced efficacy of multi-molecular collisions in generating induced dipoles. The change from free (moderately compressed gas), to strongly hindered (liquid), rotation in propyne appears as a shift to higher frequency of the absorption band observed in this case.

The exceptionally well defined near-neighbouring molecular alignment in the nematic (and, indeed, the isotropic) phase of N-(p-methoxybenzylidene)-p -n-butylaniline (MBBA) offered an interesting test for the Brot-Larkin and Wyllie-Larkin models of librational relaxation in condensed (non-gaseous) phases. Qualitative and quantitative aspects showed the 130 cm^{-1} absorption observed in this species to arise from the librational mode about its long axis. This appraisal was supported by a priori calculations of this librational barrier height. The role of molecular symmetry in relation to these barriers has been illustrated by a comparison of substituted ethanes with molecules forming rotator phases.

Equations for digital computation have been developed for multipole induced dipolar absorption in bimolecular collision of symmetric top and linear molecules, using Frost's general theory.

CONTENTS

C H A P T E R 1

General Introduction

In general, this thesis aims to illustrate the proposition that original and detailed information on molecular dynamics and interactions in the compressed gaseous and liquid state can be gleaned from observations of their absorptions in the far infra-red region of the electromagnetic spectrum.

The far infra-red is usually accepted as that region from about $\bar{\nu}$ = 2 cm^{-1} (λ = 5 mm) to about 400 cm^{-1} (0.025 mm). It is the high frequency adduct of the microwave region, extending into the conventional infra-red. The absorptions studied for this thesis were either high frequency parts of those resonant and non-resonant processes occurring in the microwave region, or low frequency infra-red resonant type absorptions such as those arising from rotational movements of small molecules. These observations have been classified below.

(I) Pure Rotational Motion of Small Polar Molecules.

As is very well-known, a solution of the Schrödinger equation for pure rotational motion in the simplest case of a diatomic polar molecule such as (H - F) indicates that the rotating molecule inhabits a series of energy levels given by $E_J = \bar{B}\, J(J + 1)$, where J is the pure rotational quantum number and $\bar{B}$ is the rotational constant in wavenumbers (cm^{-1}). The wave equation predicts that absorptions are allowed from E(J) to E(J + 1) only, resulting in a series of lines at $\bar{\nu} = 2\bar{B}(J + 1)$ separated by the constant wavenumber value $2\bar{B}$. The lines are of relative intensity governed by a Boltzmann population distribution. This Boltzmann distribution of lines is what is observed in the far infra-red at pressures of $\leq$ 1 m bar, with high resolution, although the spacing is not the constant $2\bar{B}$ because of the slight stretching of the diatomic or linear molecule on rotation. At higher pressures (up to 1 bar) and/or with decreased resolution (about 4 cm^{-1}),

the lines merge due to collisional broadening into their Boltzmann profile, and all that can be observed is the bell-shaped band. In some special cases, such as those of almost spherical small dipolar molecules (e.g. $CClF_3$) this basic band shape is still predominant, indicating that there is almost free rotation even at the liquid molecular number density.

(II) Absorptions by Pressurised non-dipolar Gases and Liquids.

An induced infra-red absorption spectrum was first identified in 1949 (1) in compressed gaseous and liquid oxygen. The molecular rotations became infra-red active because of electric dipole moments induced in colliding pairs of molecules by intermolecular forces. The dipole moment depends in magnitude on the intermolecular distances and in direction on the orientation of the colliding molecules. The molecular pair can consequently absorb energy from a radiation field at its frequency of rotation. The intensity of a given absorption band depends on the strength of the induced dipole moment, which depends on molecular parameters such as the polarisability and the multipole moments of each molecular electric field. In principle, the lower moments such as the quadrupole can be derived from the intensity of the induced band in non-dipolar molecules.

The collision-induced rotational spectrum of hydrogen was observed in 1955 (2). It was studied in more detail by Colpa and Ketelaar (3), and by Kiss, Gush, and Welsh (4). The bands observed are very broad because the induced dipole moments exist only for the duration of the collision. It was remarked (4) that the rotational spectrum appeared to be superimposed on a continuum that decreased in intensity with increasing frequency. It was postulated that this

continuum arose from pure translational absorption, whereby the absorption of a photon changes the relative kinetic energy of the colliding molecules without changing their state of internal motion. The existence of translational absorption was demonstrated conclusively by Kiss and Welsh (5) who found an absorption in mixtures of compressed rare gases in the region between 350 and 700 cm^{-1}. The early measurements (4,6) were limited to about 350 cm^{-1} on the low frequency side, but those of Bosomworth and Gush (7) on compressed helium-argon and neon-argon mixtures, and on compressed hydrogen, nitrogen and oxygen extended the observations down to 20 cm^{-1}. They found that the far infra-red spectra in each case consisted of overlapping translational and rotational branches, except in the rare gas mixtures, where only the translational component exists. The translational branch is otherwise distinguishable only for hydrogen and CO_2. In the case of oxygen and nitrogen, the spacing between the rotational lines is smaller and the two branches overlap completely.

More recently, Ho, Birnbaum and Rosenberg (8) have made accurate measurements of the collision-induced absorption in carbon dioxide at a number of temperatures in the range 233 - 333K and in the frequency region 7 - 250 cm^{-1}. They obtained direct evidence for the separation of the pure translational and the rotational-translational bands at all temperatures. Collision-induced translational absorption had been observed previously from microwave measurements of compressed CO_2 (9), which is a particularly favourable case for this kind of study because the spectrum, which arises from the dipole moment induced in interacting CO_2 molecules primarily by the quadrupole moments of their fields, is particularly intense because the quadrupole moment of CO_2 is large (10). These authors

also made a careful study of the pressure dependence of the collision-induced spectrum in CO_2 at room temperature in the same frequency region. One of the most characteristic features of collision-induced spectra is the dependence on molecular number density N (molecules cm^{-3}) of its integrated absorption intensity $A = \int_0^\infty \alpha(\bar{\nu})\, d\bar{\nu}$, where $\alpha(\bar{\nu})$ is the absorption coefficient per unit length (cm). At low densities A is proportional to N^2 because two molecules are required for the production of an induced dipole. (The band shape is independent of density because the induced dipole persists only for the duration of collision, provided that intercollisional correlation effects are negligible). At higher densities, however, the integrated absorption is observed to increase less rapidly than N^2, and, provided the density is not too great, can be represented by a term which varies as N^3. Carbon dioxide shows a departure from an N^2 dependence which can be represented by a rather large negative contribution varying as N^3.

Band shape changes were also observed, and to explore this further, they (8) investigated the far infra-red spectrum of liquid CO_2 at 273K. They found that the peak intensity in the liquid compared with that obtained in the gas phase at the same temperature had shifted by about 25 cm^{-1} to a higher frequency. In addition, A/N^2 in the liquid was about 25 times smaller than that in the low density gas, a result which was interpreted to reflect a cancellation of a large part of the induced dipole moment due to the ordered nature of the liquid state: Bose and Cole (11) having previously pointed out that collision-induced absorption in liquid CO_2 would disappear if each molecule occupied a site of inversion symmetry. Despite the reduction in the induced dipole moment, the molecules in the liquid are subject to

powerful intermolecular forces because of the shift in the peak of the absorption curve by 25 cm^{-1}. Treating their data via the equation $\alpha(\bar{\nu},N) = \alpha_2(\bar{\nu})N^2 + \alpha_3(\bar{\nu})N^3$, where $\alpha_2(\bar{\nu})$ and $\alpha_3(\bar{\nu})$ are the induced coefficients due to binary and ternary interaction respectively, and examining the ratio $\alpha_3(\bar{\nu})/\alpha_2(\bar{\nu})$, Birnbaum, Ho, and Rosenberg concluded that the high frequency (>150 cm^{-1}) wing of the CO_2 absorption is due entirely to two-body interactions. They tentatively attributed this absorption to short-range interactions giving rise to dipole induction by an overlap process or via the hexadecapole moment (10). They estimated that A/N^2 from 150 cm^{-1} to higher frequencies in CO_2 was very roughly about 5% of the total; and also that A/N^2 in the liquid was about 4% of the low density gas value, which led to the speculation that the part of the dipole moment due to quadrupolar induction was effectively cancelled in the liquid, leaving essentially the contribution from shorter-range interactions. In the case of SF_6 (12), where the induction is thought to arise predominantly from the hexadecapole moment, A/N^2 is essentially the same in the gas and the liquid.

Part of the work for this thesis was to study the molecular interactions causing a far infra-red absorption in compressed gaseous and liquid cyanogen, $(CN)_2$, a non-dipolar linear molecule with a very large quadrupole moment (13). The absorption was studied in the region 20 - 100 cm^{-1} at pressures of up to 33.5 bar, together with a liquid spectral study at 301K in the same region. From the integrated intensity of the gaseous absorption, an apparent quadrupole moment was computed. For the liquid an apparent molecular quadrupole moment was deduced, the much loger value of which reflected inter alia the reduced efficacy of multi-molecular collisions in generating dipoles,

a trend similar to that observed for CO_2. An interesting feature of this study was the discrepancy found between the observed $\tilde{\nu}$(max) of the compressed gas spectrum and the corresponding theoretical $\tilde{\nu}$(max) calculated using an equation derived by Colpa and Ketelaar (14). This type of discrepancy has been observed (7) for oxygen, and is probably due to short-range binary interactions similar to, but much more intense than, those observed in carbon dioxide described above.

(III) Absorptions by Compressed Dipolar Gases

In addition to induced dipolar absorptions there is, of course, a contribution from the permanent dipole moment, which is predominant except in the case of N_2O (15). The pure dipolar contribution to A can be conveniently estimated using a sum rule due to Gordon (16), who estimated the total optical absorption due to a system of rigid molecules of arbitrary mass and charge distribution. For uncharged molecules which have random orientations, the sum rule reduces to:

$$A = \int_0^\infty \alpha(\tilde{\nu})\, d\tilde{\nu} = \frac{N\pi}{3c^2}\left[\frac{\mu_y^2+\mu_z^2}{I_x} + \frac{\mu_x^2+\mu_z^2}{I_y} + \frac{\mu_x^2+\mu_y^2}{I_z}\right] \quad (1)$$

where Ix, Iy and Iz are the principal moments of inertia of the molecule, and μ_x, μ_y, and μ_z are the components of the dipole moment along these axes. For symmetric tops or linear molecules, Ix = Iy = I, and:

$$A = \frac{2\pi N \mu^2}{3c^2 I} \quad (2)$$

where μ is the dipole moment in a direction perpendicular to that about which I is calculated.

Induced absorptions are not accounted for in this sum rule, and the ''internal field'' effect present in dipolar liquids and solids must be allowed for by a correction such as that of Polo and Wilson (17) which gives the absorption (A) when the refractive index of the medium is 1.0, corresponding to the liquid integrated intensity A_l:

$$A = \frac{9n}{(n^2 + 2)^2} \cdot A_l \qquad (3)$$

where n is ideally the frequency dependent refractive index in the far infra-red, but which is often approximated by the D-line index n_D.

Another part of this thesis was the study of the near-linear, dipolar molecule propyne (18) in the compressed gaseous, liquid, and solution states in the frequency range 10 - 200 cm^{-1}. The purpose of this study was to estimate the extent of dipole induction in the compressed gas, and to compare these latter absorption contours with that of the liquid. Recent studies in the far infra-red have shown that all polar liquids have a notable broad absorption extending to about 100 - 200 cm^{-1} which has been associated with a more or less hindered rotational mode (see below). In some instances it has been possible to compare the liquid absorption with the corresponding rotational spectrum of the gaseous state and to evaluate not only the total effective dipole moment participating but also to estimate the quadrupole moment which appears to contribute. It was found that there was a considerable shift in $\bar{\nu}$ max, the frequency of maximum absorption, from 18 cm^{-1} in the gas at 5.1 bar to 81 cm^{-1} in the liquid. This shift was interpreted as being due to the change from largely free, to strongly hindered rotation. An estimate was also

made of dipole induction in liquid phase propyne-carbon tetrachloride collisions.

(IV) Absorption in Dipolar Liquids.

Spectroscopic methods such as those concerned with the near infra-red region observe absorptions due to changes within the quantised energy levels of a molecule, but dielectric spectroscopy in the region of lower frequency than the far infra-red is concerned with the motion of the whole molecule, giving us an insight to the immediate surroundings and molecular dynamics in the liquid state. In the dielectric dispersion region, what one can see is an absorption due to the rate at which the molecule can turn around, this being a cooperative process, and not one arising from the motion of a particular molecule in isolation.

Debye's model (19) of the rate of dipole reorientation in the liquid state was based on the rotation of a rigid molecule with a viscous drag leading to a constant angular velocity ω. On removal of a static field at t = o, the dipole polarisation decays with an unique rate coefficient:

$$P(t) = P(o)\exp(-kT) = P(o)\exp(-t/\tau) \quad (4)$$

The Debye relations then follow:

$$\epsilon'' = (\epsilon_o - \epsilon_\infty)\omega\tau/(1+\omega^2\tau^2) \quad (5)$$

$$\epsilon' = \epsilon_\infty + (\epsilon_o - \epsilon_\infty)/(1+\omega^2\tau^2) \quad (6)$$

These are sufficiently accurate for most polar liquids, and occur over a range of frequencies where the dielectric constant, or

permittivity, falls from its value ϵ_0 when a static field is applied to ϵ_∞ where the molecules are no longer able to follow the high frequency oscillation of the applied field.

After a careful study of the difference between his ϵ_∞ values and Cartwright and Errera's (20) values for n_{ir}^2, the square of the far infra-red refractive indices, for a series of substituted benzenes, Poley (21) predicted an absorption for polar liquids in the very far infra-red, i.e. there must be a further dispersion region beyond the Debye range of $(\epsilon_0 - \epsilon_\infty)$ due to some very fast movement of the whole molecule. Examining (5) at frequencies where $\omega\tau \gg 1$, then:

$$\epsilon'' = (\epsilon_0 - \epsilon_\infty)/\omega\tau \qquad (7)$$

and using the well-known relation:

$$\alpha(\bar{\nu}) = 2\pi\epsilon''(\bar{\nu}).\bar{\nu}/n(\bar{\nu}) \qquad (8)$$

$$\text{then } \alpha\,(\text{Debye limit}) = (\epsilon_0 - \epsilon_\infty)/n(\bar{\nu})c \qquad (9)$$

Taking $n(\bar{\nu})$ as varying by not more than $\pm$ 10% between the far infra-red and the visible, then equation (9) predicts a strong absorption by all polar liquids throughout this frequency range. The anomaly arises from Debye's equation of motion:

$$-\underline{\mu} \times \underline{F} = -\mu F \sin\theta = \zeta \frac{d\theta}{dt} \qquad (10)$$

where $\underline{\mu} \times \underline{F}$ is the torque on a dipole exerted by an external field $\underline{F}$. The angular velocity $\dot{\theta}$ is assumed to be proportional to the couple on the dipole through ζ, which describes the microscopic viscous drag on the molecule. However, (10) does not include the term $I\ddot{\theta} = I\dot{\omega}$ which arises from the molecular inertia, the neglect of this term having serious spectral consequences only at frequencies

of about 10 cm^{-1} and higher.

A solution of the equation:

$$-\underline{\mu} \times \underline{F} = \zeta \dot{\theta} + I \ddot{\theta} \qquad (11)$$

leads (22,23) to spectral transparency typically at about 100 cm^{-1} after a period of approximate constancy in $\alpha(\bar{\nu})$ lasting from about 10 - 100 cm^{-1}, known as the Debye absorption plateau level.

One of the first liquids to be studied in the far infra-red was the pseudo-spherical 1,1,1 trichloroethane ($CH_3.CCl_3$). This was chosen (24) because it has $\epsilon_\infty \doteq n_{ir}^2$ and is a good approximation geometrically to the modified Debye model treatment of equation 11, in which the dipole is placed at the centre of a polarisable sphere. However, the experimental A/N was found to be much greater than that predicted by dynamics such as those of (11). This excess was subsequently (25, 32) found to be typical of dipolar liquids; a representative absorption band having the following properties.

(i) It is broad, $(\Delta\bar{\nu})_{1/2} \doteq 50$ cm^{-1}, and featurless.

(ii) $\alpha(\bar{\nu}) \propto N$, as established by dilution with non-dipolar solvents.

(iii) $\bar{\nu}(max)$ is usually increased by a decrease in temperature.

(iv) The refractive index goes through a minimum corresponding to a maximum in $\alpha(\bar{\nu})$. Thus the absorption is associated with some process occurring at a specific frequency, or range of frequencies.

Recently, two models have been developed (26, 27) which have attempted to describe this experimental excess, or "Poley absorption" in terms of libration, or torsional oscillation, of whole molecules

constrained by the energy barriers due to the fields of this central molecule's rather close packed neighbours. This high frequency process occurs simultaneously with the lower frequency Debye dynamics described by (11) which represents the cooperative part of the relaxation process. The overall molecular motion is separated into a Debye part and a Poley part for convenience. Both models consider the ''excess'' absorption in terms of librational motion of a dipolar molecule of inertia I within a potential well of depth V and semi-angular aperture ξ due to its nearest neighbours. The well is given the arbitrary form:

$$U(\theta) = V \sin^2 (\pi\theta/2\xi) \qquad (12)$$

giving a harmonic (small angle) solution of the form:

$$\omega_o = \frac{\pi}{\xi}\left(\frac{V}{2I}\right)^{1/2} \qquad (13)$$

Although a distribution of potential well depths and shapes is expected giving a distribution of fundamental librational frequencies ω_o, a system of identical wells restricts the number of unknown parameters in the final expression for $\alpha(\bar{\nu})$.

Model I: Autocorrelation Function Treatment of a Librator in a Multi-Well Potential.

This model was originally proposed by Brot et. al. (28) for plastic crystals and liquids with a quasi-crystalline structure, libration of a dipole within a parabolic potential well (or the symmetric potential of (12)) being perturbed by ''weak'' thermal collisions of mean frequency $1/\tau_i$, while ''strong'' collisions (of frequency weighted by a Boltzmann factor) induce relaxational jumps from one well to another.

The duration of jump τ_j is taken to be the mean time of jump (evaluated by numerical integration of the motion of a molecule) as a

function of energy in excess of the barrier height V, weighted by a Boltzmann distribution: the resulting τ_j is only slightly dependent on V, but is a function of well shape, angular aperture, and moment of inertia of a molecule, I, the incidence of the latter resulting in the return to transparency at high frequency.

Brot's arbitrary correlation function of the jumping molecule:

$$H(t) = (1 + t/\tau_a)\exp(-t/\tau_a) \qquad (14)$$

then defines parameter τ_a, because, when $t = t_j$

$$H(t_j) \doteq \langle \cos \theta_j \rangle \qquad (15)$$

where the mean angle of jump $\theta_j \doteq (2 \pm 1)\xi$ for intermediate values of τ_i, the case where thermal collisions stabilise the molecule in the next potential well (29).

The mean time of residence of a librator within a well is determined by the ratio of the number of molecules within a well to the number jumping,

$$\tau_i / \tau_j = (1 - \exp(-V/kT))/\exp(-V/kT) \qquad (16)$$

where $\tau_r \doteq \tau_D$, the Debye relaxation time.

The halfwidth at half maximum of the librational absorption is represented empirically as:

$$\frac{1}{\tau} = \frac{\omega_o}{4} + \frac{\pi}{\tau_i} \qquad (17)$$

where the first term on the right hand side reflects the anharmonicity of the potential well function $U(\theta)$, the fact that the actual potential well will not, in general, be of the assumed cylindrical symmetry, and that a distribution of well shapes and/or depths is expected.

The second term is the result of the uncertainty principle and collisional perturbation of the librator, where $\tau_i = \tau_j$. The values of $1/\tau_i$ obtained from fitting observed spectra with (17) are, of course, merely "apparent" collision frequencies.

If cross-correlation terms and internal field are neglected, the relation obtained is (28):

$$\frac{\epsilon^* - \epsilon_\infty}{\epsilon_0 - \epsilon_\infty} = 1 - i\omega \mathcal{F}(i\omega) \qquad (18)$$

where the Laplace transforms of the librational auto-correlation function (30):

$$\mathcal{V}(i\omega + 1/\tau_r) = \frac{(i\omega + 1/\tau_r + 2/\tau)}{-\omega^2 + \omega_0^2 + 1/\tau_r^2 + 2i\omega(1/\tau + 1/\tau_r) + 2/\tau_r\tau} \qquad (19)$$

and that of the jumping molecule:

$$\mathcal{H}(i\omega) = \frac{i\omega + 2/\tau_a}{-\omega^2 + 1/\tau_a^2 + 2i\omega/\tau_a} \qquad (20)$$

give the Laplace transform of the combined autocorrelation function:

$$\mathcal{F}(i\omega) = \left[\frac{1 - 2\beta^2}{i\omega + 1/\tau_r} + 2\beta^2 \mathcal{V}(i\omega + 1/\tau_r)\right]\left[1 + \frac{\mathcal{H}(i\omega)}{\tau_r}\right] \qquad (21)$$

where $\beta^2 = kT/I\omega_0^2$.

Thus, $\alpha = \epsilon''\omega/nc \propto Re\left[F(i\omega)\right] \to 0$ as $\omega \to \infty$. The approximate proportionality constant, neglecting internal field effects, is: $(\epsilon_0 - \epsilon_\infty)/nc$.

An experimentally observed spectrum is fitted by deducing a value for the aperture angle ζ from the lattice structure of the rotator phase solid or from the "coordination number", i.e. the number of nearest neighbours characterising the immediate local order around a molecule in the liquid (31). Trial values of V and τ_i

are used in a calculation of the absorption spectrum, these values being adjusted to obtain the best fit to ω_o, $\tau_r = \tau_D$, and the relative amplitude of librational and relaxation absorptions. The prediction (32) that a potential well may become narrower on cooling, and the decreasing amplitude of motion of the librator's neighbours, may be approximated simply by:

$$u(\theta) = V \sin^2(\pi\theta/2\xi_1), \quad 0 \leq \theta \leq \xi_1/2 \qquad (22)$$

where $\omega_o = \frac{\pi}{\xi_1}\left(\frac{V}{2I}\right)^{1/2}$ (22a)

and $$u(\theta) = V \sin^2\left(\frac{\pi(\theta + \xi - \xi_1)}{2(2\xi - \xi_1)}\right) \qquad (23)$$

which reduces to (12) when $\xi = \xi_1$. This arbitrary form has been used for ease of calculation, the narrower lower portion (22) defining the librational motion (22a) while the aperture ξ remains constant. This more complicated well shape is used if the calculated $\tau_r \gg \tau_D$ and/or $\omega_o(\text{calc.}) \ll \omega_o(\text{obs.})$, in which case a trial value of $\xi_1 \lesssim \xi$ may be used in the calculations, the parameters again being adjusted to obtain a good fit to the observed spectrum. For ease of line-shape comparison, the calculated spectra are normalised to the observed maximum absorption.

Model II: The Itinerant Oscillator.

This model was originally proposed by Hill (33) for a librator of moment of inertia I within a "temporary cage" of Z nearest neighbours of moment of inertia I_c in the liquid state: the damping (r) of the librator was assumed not to be of a collisional nature, but to arise from lack of rigidity of the cage. Debye relaxational absorption occurs through the cooperative diffusional reorientation of the

cage molecules about their centres of mass against a resistence ζ. Wyllie (34), using the equations of motion (24) and (25) included the inertial effect of the cage on the relaxational absorption with the required return to transparency at high frequencies, but set the damping factor $I(r)$ of the librator to zero. Larkin (27) included both the inertial and damping terms in the model, giving the equations:

$$I_c\ddot{\alpha} + \zeta\dot{\alpha} - I\omega_o^2\phi = M(t) \qquad (24)$$

$$I\ddot{\theta} + I_r\omega_o\dot{\phi} + I\omega_o^2\phi = -\mu E'\sin\theta + L(t) \qquad (25)$$

where $E' = E\exp(i\omega t)$ is the applied field defining the polar axis with respect to which $\alpha = \bar{\alpha} + A\exp(i\omega t)$ defines the mean position of the dipole μ, $\theta \equiv (\phi + \alpha)$ the instantaneous position, and hence $\phi = (\theta - \alpha) \equiv \Phi\exp(i\omega t)$ the instantaneous polar deviation and response to the applied field. $L(t)$ and $M(t)$ are stochastic functions of mean zero, which are replaced (after Debye and Hill) by an appropriate rotary diffusion. The equations of motion are solved (assuming $\omega \ll \omega_o$ and $\mu E \ll kT \ll I\omega_o^2$) to give the Fick diffusion equation from which a solution of the dipole moment distribution function, $f(\theta)$, is obtained. The mean dipole moment parallel to the field (and hence the frequency dependent polarisability) then give the optical coefficient $\alpha(\omega)$.

Before fitting calculated to experimental spectra, an estimate of the well aperture ξ must be made from X-ray data of the solid or rotator phase (where applicable), from molecular symmetry, or coordination number in the liquid state via (27):

$$\xi \lesssim \tan^{-1} a\left[(1-Z^{-1})/Z\right]^{1/2}/(1-a/Z) \qquad (26)$$

A potential well is then chosen to fit the observed frequency of maximum excess absorption, a value of ζ being chosen from:

$$\tau_D = \zeta / 2kT \qquad (27)$$

to fit the observed Debye relaxation time $\tau_D \doteq \tau_d$ (the diffusion time of the cage). Spectra may then be calculated with these trial values of V, ζ, and r (chosen to fit the width of the librational absorption) and these parameters adjusted to give the best overall fit. If ''narrowed'' wells are used in this model, the librational frequencies would be held constant by choosing a new value of V from (22a), other parameters being unchanged.

Another part of this thesis consisted of interpreting microwave and far infra-red absorption of some dipolar liquids in terms of librational and relaxational motion using these two models. The spectra of 1,2-dibromo-1,1-dichloroethane; 1,2-dibromo-2-methylpropane; 1-iodo-2-methylpropane, and 1-iodo-3-methylbutane obtained by Moisan (35) were fitted using both models. An acceptable fit (36) to the observed data was obtained on the assumption of a hexagonal symmetry for the planar disposition of the potential wells. The barrier heights to libration suggested by this phenomenological approach were, as expected, greater than results for molecules of enhanced symmetry (26) which form rotator phases.

(V) Absorption by the Nematic and Isotropic Phases of Liquid Crystals.

The nematic phase of a liquid crystal offered a particularly interesting situation in which to test these models further. A liquid crystal is characterised by the tendency of molecules to lie with their long axes parallel even when they are separated by long distances. This conclusion is associated with the essentially normal permittivity of the nematic liquid in relation to the effective resultant electric moment of the monomer molecules of the liquid crystal.

The species studied for this thesis was N-(p-methoxybenzylidene)-p-n-butylaniline or MBBA (31). Qualitative and quantitative aspects showed the 130 cm^{-1} absorption in this species to arise from the librational mode about the long axis of the MBBA molecules. The contour of the absorption (including that of the microwave region) is fitted in terms of both these models with closely comparable apparent energy-well depths (16 to 19 kJ $mole^{-1}$). This appraisal was supported by an a priori calculation of the form and depth of the energy wells in terms of the parameters established for phenyl-ring interactions in the Rae-Mason evaluations (37) of the lattice energy of benzene.

CHAPTER 2

Experimental

The absorption intensity measurements in the region 10 - 200 cm^{-1} were carried out with a Grubb-Parsons/N.P.L. cube interferometer (38-41) with amplitude modulation of the radiation from a high-pressure-mercury broad band source (see below). The first part of this chapter will deal with the theory of Michelson interferometry, and the second will describe in detail the instrumentation, purification techniques, and sample cells used.

Theory of Interferometry.

Basic Principle.

The instrument is based on the operation of a Michelson two-beam interferometer (fig.2.1). A parallel beam of radiation from the source (S) is split by a beam divider (B) (which is usually a thin, transparent sheet of polyethylene terephthalate) into two perpendicular beams. These are reflected off front-aluminised mirrors M_1 and M_2, and after recombination at the beam divider the emergent beam is focused onto a detector. This basic optical instrument is operated by altering the geometric path length difference between the two arms of the interferometer, i.e. by moving one mirror backwards or forwards along the radiation axis.

Considering the interferometer illuminated by monochromatic radiation of frequency ν then if $OM_1 = OM_2$, where O is the mid-point of the beam divider on the optical axis, the two branches of radiation from the mirror will recombine at the beam divider in phase, and the signal at the detector (D) will be a maximum. If the path-length in one arm is increased by moving the mirror back, the signal at the detector will decay, and at a certain position of the movable mirror

will become minimal. In this condition, the two beams are interfering destructively. Thus, for monochromatic radiation, the signal at the detector will rise and fall periodically:

$$Io(x) = Io \cos (2\pi \bar{\nu} x) \qquad (1)$$

here Io is the maximum intensity (for $OM_1 = OM_2$), x is twice the mirror displacement, and $\bar{\nu}$ is the wavenumber of the monochromatic source. Io(x) is the interferogram function.

Polychromatic, or broad band radiation (such as that from a high-pressure-mercury arc source) can always be looked upon as an assembly of monochromatic lines, and the corresponding interferograms will be simply a combination of functions such as (1) with different amplitudes and wavelengths, and will have the form:

$$I(x) = \int_{-\infty}^{\infty} G(\bar{\nu}) \cos(2\pi \bar{\nu} x) d\bar{\nu} \qquad (2)$$

where G is a function of $\bar{\nu}$, and measures intensity, and is thus a spectral function. By placing a sample (A) between the emergent beam and the detector, $G(\bar{\nu})$ will be altered in (2) (since A will absorb some frequencies from the polychromatic radiation), and thus I(x) will also alter. By Fourier's integral theorem:

$$G(\bar{\nu}) = \int_{-\infty}^{\infty} I(x) \cos(2\pi \bar{\nu} x) dx \qquad (3)$$

Thus, in principle, $G(\bar{\nu})$ may be obtained from a knowledge of the interferogram function I(x), (fig.2.2).

General Theory of Fourier Transform Spectrometry (42)

Following Chamberlain's treatment (42) the power $I_o(x)$ in the interference pattern produced at the exit stop of a two-beam (Michelson) interferometer (fig. 2.3), within which there is a geometrical path difference x, is the sum:

$$I_o(x) = I_o + F_o(x) \qquad (4)$$

of a constant term: $I_o = \int_{-\infty}^{\infty} P_o(\bar{\nu})d\bar{\nu} \quad (= \bar{I}_o(x)) \qquad (5)$

and an x dependent term:

$$F_o(x) = \int_{-\infty}^{\infty} P_o(\bar{\nu})\cos(2\pi\bar{\nu}x - \Phi_o(\bar{\nu}))d\bar{\nu} \qquad (6)$$

called the interferogram function.

$P_o(\bar{\nu}) = \frac{1}{2}\tau_1(\bar{\nu})\mathcal{L}(\bar{\nu})$ is the (even part of the) power spectrum of the detected radiation of wavenumber $\bar{\nu}$; $\mathcal{L}(\bar{\nu})$ is the (even part of the) power spectrum of the radiation incident on the interferometer, and $\tau_1(\bar{\nu})$ is the transmission factor of the interferometer. $\Phi(\bar{\nu})$ is the phase difference due to any residual asymmetry in the interferometer.

When a plane-parallel, isotropic specimen of thickness d, transmissivity $\tau(\bar{\nu})$, and refractive index $n(\bar{\nu})$ is placed before the detector of the interferometer, the expression for the centre power becomes:

$$I(x) = I + F(x) \qquad (7)$$

where $I = \int_{-\infty}^{\infty} P(\bar{\nu})d\bar{\nu} = (\bar{I}(x)) \qquad (8)$

$$F(x) = \int_{-\infty}^{\infty} P(\bar{\nu})\cos(2\pi\bar{\nu}x - \Phi_o(\bar{\nu}))d\bar{\nu} \qquad (9)$$

and $P(\bar{\nu}) = \tau(\bar{\nu})P_o(\bar{\nu}) \qquad (10)$

Applying Fourier's inversion theorem to (6) and (9), we find the complex spectra:

$$\hat{S}_o(\bar{\nu}) = P_o(\bar{\nu})_e{}^{-i\Phi_o(\bar{\nu})} = P_o(\bar{\nu}) - iQ_o(\bar{\nu}) = \int_{-\infty}^{\infty} F_o(x)_e{}^{-2\pi i \bar{\nu} x}\, dx \qquad (11)$$

$$\hat{S}(\bar{\nu}) = P(\bar{\nu})_e{}^{-i\Phi_o(\bar{\nu})} = P(\bar{\nu}) - iQ(\bar{\nu}) = \int_{-\infty}^{\infty} F(x)_e{}^{-2\pi i \bar{\nu} x}\, dx \qquad (12)$$

respectively, where each has been shown split into real and imaginary parts corresponding to the cosine and sine transforms $P(\bar{\nu})$ and $Q(\bar{\nu})$.

Synchronous Detection

The complex spectra (11) and (12) can be calculated when the (real) interferograms $F_o(x)$ and $F(x)$ are known. These are usually aperiodically scanned at a constant speed $v = dx/dt$, where t is the observation time, and recorded using amplitude modulation of the total detected signal followed by synchronous amplification. In this, the periodically fluctuating detector output is amplified and filtered, and then mixed with a reference signal derived from the modulation process. This procedure leads to a d.c. output from the amplifier (fig. 2.4) that is directly related to the peak-to-peak detector output. The great advantage is separation of the required signal from unwanted noise.

In the general case, the radiation $J(y)$ is modulated at a frequency f to give at any instant t a signal $J(y,ft)$ which can be expressed as a Fourier series:

$$J(y,ft) = \tfrac{1}{2}K^o(y) + \sum_{l=1}^{\infty}(K^l(y)\cos 2\pi l ft + Z^l(y)\sin 2\pi l ft) \qquad (13)$$

where $K^l(y)$ and $Z^l(y)$ are the Fourier coefficients. We can choose the time origin so that $J(y,ft)$ is either even or odd with respect to t. Arbitrarily choosing the odd case, then:

$$J(y,ft) = \sum_{l=1}^{\infty} Z^l(y)\sin(2\pi l\, ft) \qquad (14)$$

The output from the detector (assumed linear) is $uJ(y,ft)$, where u is the responsivity (signal delivered per unit power output). The detector signal is amplified with a gain g and passed through a filter tuned to the frequency f to give:

$$D(y,ft) = guZ^1(y)\sin 2\pi ft \qquad (15)$$

(the filter is assumed to offer no attenuation or phase shift at the frequency f). In a synchronous recording it is this signal that is multiplied and phase-locked with a reference signal, also of frequency f. A suitable signal is the (odd) square switching function of period $T_o = 1/f$, defined by:

$$R(ft) = \begin{cases} 1 & o < t < (To/2) \\ -1 & (To/2) < t < To \end{cases}$$

$$R(ft + mfTo) = R(ft); \quad m = \pm 1, \pm 2, \ldots..$$

of which the Fourier series is: $\frac{4}{\pi} \cdot \sum_{l=o}^{\infty} \left(\sin\left[2(2l+1)\pi ft\right]/(2l+1)\right)$

The result of the signal multiplication is:

$$M(y,ft) = \frac{4gu\, Z^1(y)\sin(2\pi ft)}{\pi} \cdot \sum_{l=o}^{\infty} \frac{\sin\left[2(2l+1)\pi ft\right]}{2l+1}$$

$$= \frac{4gu\, Z^1(y)\sin(2\pi ft)}{\pi} + \sum_{l=1}^{\infty} \frac{4gu\, Z^1(y)\sin\left[2(2l+1)\pi ft\right]}{(2l+1)\pi}$$

$$= \frac{2}{\pi} gu\, Z^1(y)(1 - \cos(4\pi ft)) + \ldots.$$

which consists of one nearly d.c. term:

$$V(y) = \frac{2}{\pi} gu\, Z^1(y) \qquad (16)$$

that is proportional to $Z^1(y)$, and a series of time dependent terms of frequencies that are multiples of f. A suitable low pass filter removes these to give V(y) as the synchronously amplified and rectified output signal that is recorded. (It is assumed that the signal is not subject to distortion on undergoing the convolution $V(t)*R(t)$ with the impulse response function of the filter, R(t).) $Z^1(y)$ is the coefficient of the fundamental term in the series expansion (13) of J(y,ft) and it depends on the type of modulation employed. $Z^1(y)$ is called the fundamental coefficient, and V(y) the recorded signal (differing only by the constant $2gu/\pi$).

Amplitude Modulation (A.M)

In this case, the detected radiation is:

$$Ja(y,ft) = a(ft)J(y) \qquad (17)$$

where $a(ft) = \sum_{\ell=0}^{\infty} a^{\ell} \sin(2\pi \ell ft)$ (18)

(compare (14))

is the odd modulating function. The detector output is $u\, J_a(y,ft)$, and the filtered signal to be multiplied with R(t) is:

$$Da(y,ft) = g_a\, u\, Z\dot{a}(y) \sin(2\pi \ell ft) \qquad (19)$$

(compare (15))

where $Z\dot{a}(y) = a^1 J(y) = a^1 J + a^1 G(y)$ (20)

is the A.M. fundamental coefficient and a^1 is the A.M. interferogram. The recorded signal:

$$Va(y) = \frac{2ga\, u}{\pi} a^1 J(y) \qquad (21)$$

is proportional to the total power J(y) incident on the detector.

From (20) and (21), $W_a(y)$ being defined as

$$V_a(y) - V_{\bar{a}} = \frac{2}{\pi} g_a \, u \, a^1 G(y) \tag{22}$$

is the A.M. recorded interferogram, where $V_a = (2/\pi) g_a \, u \, a^1 J$.

Applying Fourier's inversion theorem, then:

$$\hat{B}_a(\bar{\nu}) = \int_{-\infty}^{\infty} \left[V_a(y) - V_a \right] \exp(-2\pi i \bar{\nu} y) dy = \frac{2}{\pi} g_a \, u \, \hat{S}_a(\bar{\nu}) \tag{23}$$

for the calculated spectrum $B_a(\bar{\nu})$ in terms of the A.M. spectrum:

$$\hat{S}_a(\bar{\nu}) = a^1 \hat{S}(\bar{\nu}) \tag{24}$$

(compare $Z_a^1(y) = a^1 J(y)$).

Sinusoidal Amplitude Modulation

In this case $a(ft) = \frac{1}{2}(1 + \sin 2\pi ft)$

$$a^1 = \tfrac{1}{2}$$

So, using (23) and (24),

$$\hat{B}_a(\bar{\nu}) = \frac{2 g_a}{\pi} u \, \hat{S}_A(\bar{\nu}) = \frac{2}{\pi} . g_a u . \frac{1}{2} \hat{S}(\bar{\nu})$$

$$\hat{B}_a(\bar{\nu}) = \frac{g_a u . \hat{S}(\bar{\nu})}{\pi} \tag{25}$$

In all the work using the Michelson interferometer, a two-sided interferogram, as shown in fig (2.2) was measured, and the complex transform (12) evaluated. The transmitted power spectrum $I(\bar{\nu})$ is calculated from:

$$I(\bar{\nu}) = \left[(P(\bar{\nu}))^2 + (Q(\bar{\nu}))^2 \right]^{\frac{1}{2}} \tag{26}$$

Thence the absorption coefficient ($\alpha(\bar{\nu})$) of a sample of thickness d is given by:

$$\alpha(\bar{\nu}) = \frac{1}{d} \log_e \frac{I_o(\bar{\nu})}{I(\bar{\nu})}$$

$$= \frac{g_a u}{g_{(a,o)} u_o} \cdot \frac{1}{d} \log_e \left[\frac{(P_o(\bar{\nu}))^2 + (Q_o(\bar{\nu}))^2}{(P(\bar{\nu}))^2 + (Q(\bar{\nu}))^2} \right]^{\frac{1}{2}}$$

with a measured gain ratio $g_a u / g_{(a,o)} u_o = g_r$.

Digital Computation

Truncation and Apodisation

In practice, the limits of integration in (11) and (12) are restricted to $-X \leqslant x \leqslant X$. This finite movement of the mirror can be expressed by multiplying $F(x)$ in (9) with a symmetric "window function" $G(x)$ (43). Taking:

$$F(x) = \int_{-\infty}^{\infty} \hat{S}(\bar{\nu}) \exp(2\pi i \bar{\nu} x) d\bar{\nu} \qquad (28)$$

then:

$$\int_{-\infty}^{\infty} F(x) G(x) \exp(-2\pi i \bar{\nu} x) dx = \hat{S}(\bar{\nu}) * \hat{T}(\bar{\nu}) \qquad (29)$$

where $\hat{T}(\bar{\nu})$ is the Fourier transform of $G(x)$ and is convoluted with $\hat{S}(\bar{\nu})$. The convolution of two functions $\hat{S}(\bar{\nu})$ and $\hat{T}(\bar{\nu})$ is:

$$\hat{S}(\bar{\nu}) * \hat{T}(\bar{\nu}) = \int_{-\infty}^{\infty} \hat{S}(u) \hat{T}(\bar{\nu} - u) du \qquad (30)$$

which is a function of $\bar{\nu}$.

The function $G(x)$ which can be used for this purpose is:

$$G(x) = \begin{cases} 1, \text{ for } -X \leqslant x \leqslant X \\ 0, \text{ otherwise} \end{cases} \qquad (31)$$

The Fourier transform of this function is:

$$T(\bar{\nu}) = 2X \operatorname{sinc}(2\pi \bar{\nu} X)$$

(where sinc(y) = (sin y)/y), therefore:

$$\hat{S}(\bar{\nu}) * \hat{T}(\bar{\nu}) = \int_{-\infty}^{\infty} \hat{S}(u) .2X \operatorname{sinc}(2\pi X(\bar{\nu} - u)du, \text{ and}$$

$$\int_{-\infty}^{\infty} F(x)G(x)\exp(-2\pi i \bar{\nu} x)dx = \int_{-X}^{X} F(x)\exp(-2\pi i \bar{\nu} x)dx$$

$$= \int_{0}^{\infty} \hat{S}(u)\ 2X \left[\operatorname{sinc}(2\pi(\bar{\nu} - u)X) + \operatorname{sinc}(2\pi(\bar{\nu} + u)X)\right]$$

(because of the symmetry of the sinc function).

Monochromatic Input

In this case, $F(x) = \cos 2\pi \bar{\nu}_o x$, and (32) holds if $\hat{S}(u)$ is a delta function, (since $\int \cos nx \cos mx\, dx = \frac{\sin(m-n)x}{2(m-n)} + \frac{\sin(m+n)x}{2(m+n)}$).

Therefore the output of a monochromatic input for finite path difference is given by $\hat{S}(\bar{\nu}_o) * \hat{T}(\bar{\nu} - \bar{\nu}_o)$, which is:

$$A(\bar{\nu}, \bar{\nu}_o) = 2X\left[\operatorname{sinc}(2\pi(\bar{\nu} - \bar{\nu}_o)X) + \operatorname{sinc}(2\pi(\bar{\nu} + \bar{\nu}_o)X)\right] \qquad (33)$$

This function has two peaks (at $\bar{\nu} = \bar{\nu}_o$, and $\bar{\nu} = -\bar{\nu}_o$). The peaks at $-\bar{\nu}_o$ and $\bar{\nu}_o$ have wings, hence the hypothetical peak at $-\bar{\nu}_o$ may reach into the region $\bar{\nu} > o$. However, if $\bar{\nu}_o \gg 1/X$, this influence can be neglected. In the far infra-red, for frequencies as low as 10 cm^{-1}, one has to choose $X \gg 1.0$ mm. $A(\bar{\nu}, \bar{\nu}_o)$ is known as the apparatus function, and neglecting the second term in (33) (which is small if $(\bar{\nu} + \bar{\nu}_o)X$ is large):

$$A' = 2X \operatorname{sinc}\left[2\pi(\bar{\nu} - \bar{\nu}_o)X\right] \qquad (34)$$

$(\Delta\bar{\nu})_{\frac{1}{2}}$ for this function is about 1/2X, and therefore depends on X inversely. The larger is X, the better the resolution, R, which is defined as the distance from the mean peak of the spectral window to the first zero. For A', R = 1/2X. However, A' has the disadvantage

of negative side lobes (which give physically meaningless negative intensities from $\hat{S}(\bar{\nu}) * \hat{T}(\bar{\nu})$). Removing or suppressing them can be accomplished by replacing the window function $G(x)$ by other functions. This process is called ''apodisation''. In this work we use the weighted function $G(x)\cos^2(\pi x/2X)$ which gives the apparatus function:

$$A''(\bar{\nu}) = \sin(2\pi X(\bar{\nu} - \bar{\nu}_o))/[2\pi(\bar{\nu} - \bar{\nu}_o)(1 - (2X(\bar{\nu} - \bar{\nu}_o))^2)] \qquad (35)$$

for monochromatic input $\bar{\nu}_o$, which has considerably reduced side lobes. The reduction is achieved, however, with a loss of resolution, and we now have $R = 1/X$.

Sampling

In order to consider the effect of sampling, the infinite Dirac comb $\amalg(x/\Delta x)$ is used. If the impulses are separated by Δx, then:

$$\amalg(x/\Delta x) \equiv \sum_{n=-\infty}^{\infty} \delta(x/\Delta x - n) = \Delta x \sum_{n=-\infty}^{\infty} \delta(x - n\Delta x) \qquad (36)$$

where δ is the Dirac delta function. The Fourier transform of $\amalg(x/\Delta X)$ is $(1/F)\amalg(\bar{\nu}/F)$, which is a sequence of impulses spaced at intervals of $F = 1/\Delta x$.

$$\int_{-\infty}^{\infty} F(x)\amalg(x/\Delta X)\exp(-2\pi i\bar{\nu}x)dx = \frac{1}{F}\int_{-\infty}^{\infty} \amalg(u/F)P(\bar{\nu} - u)du$$

$$= \int_{-\infty}^{\infty} \sum_n \delta(u - nF)P(\bar{\nu} - u)du, \text{ using (36)}$$

$$= \sum_{n=-\infty}^{\infty} P(\bar{\nu} - nF) \equiv \sum_{n=-\infty}^{\infty} P(\bar{\nu} + nF) = P_p(\bar{\nu}).$$

Therefore, transformation of a function sampled at intervals Δx leads

to a <u>periodic</u> function $P_p(\bar{\nu})$ with period $F = 1/\Delta x$, $P(\bar{\nu})$ being the real part of the interferogram function $F(x)$.

Now, if $P(\bar{\nu})$ is not chosen to be zero for $(|\bar{\nu}|) > F/2$, then the replication of the $P(\bar{\nu})$ functions leads to their overlapping, which disturbs the calculated spectrum. This problem is called aliasing, and the frequency $F/2$ is called the aliasing, folding Nyquist, or ''cut-off'' wavenumber. To avoid aliasing, Δx is chosen sufficiently small to ensure that $P(\bar{\nu}) = 0$ for $|\bar{\nu}| > F/2$ and for this the maximum frequency present in the spectrum must be known. $P_p(\bar{\nu})$ is completely specified by the range $[0, F/2]$ because of its symmetry. We divide the range $[0, F/2]$ into N intervals of width $\Delta\bar{\nu}$:

$$\Delta\bar{\nu} = F/2N = 1/2N\Delta x,$$

and then define: $2X = 2N\Delta x$ (37)

so that $2X = 1/\Delta\bar{\nu}$. $P_p(\bar{\nu})$ is now discrete, being sampled at intervals $\Delta\bar{\nu}$. We write this as $P_p(j\Delta\bar{\nu})$, $j = 0, 1, \ldots N - 1$ for the range $[0, F/2]$. We take a similar view of the imaginary part of the transform, i.e. $Q_p(j\Delta\bar{\nu})$, $j = 0, 1, \ldots N - 1$. We now define the function:

$$F_p(x) = \sum_{n=-\infty}^{\infty} F(x + m\,2X)$$

which is periodic with period $2X$. We consider this function sampled at intervals Δx, i.e. $F_p(k\Delta x)$, $k = 0, 1, \ldots 2N - 1$, giving rise to N points for $P_p(\bar{\nu})$ and N points for $Q_p(\bar{\nu})$. It can be shown that if $S = P - iQ$, then (44):

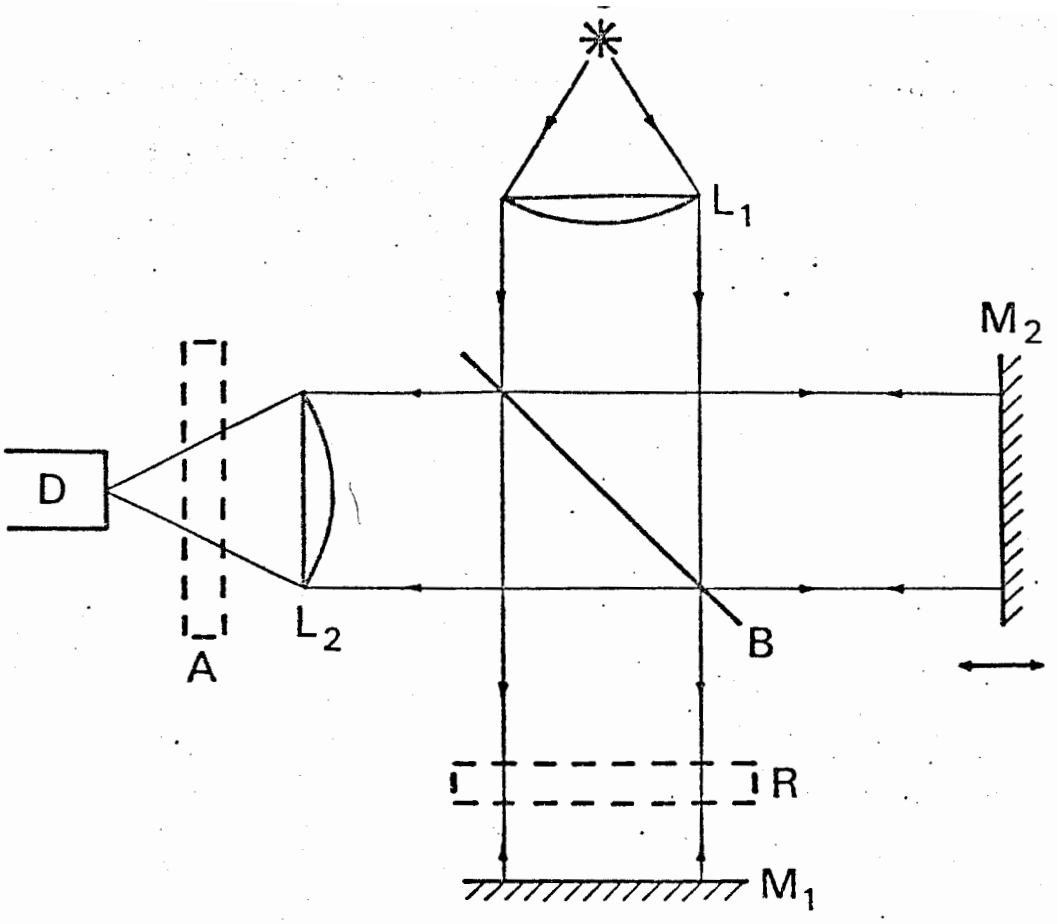

Fig. 2.1

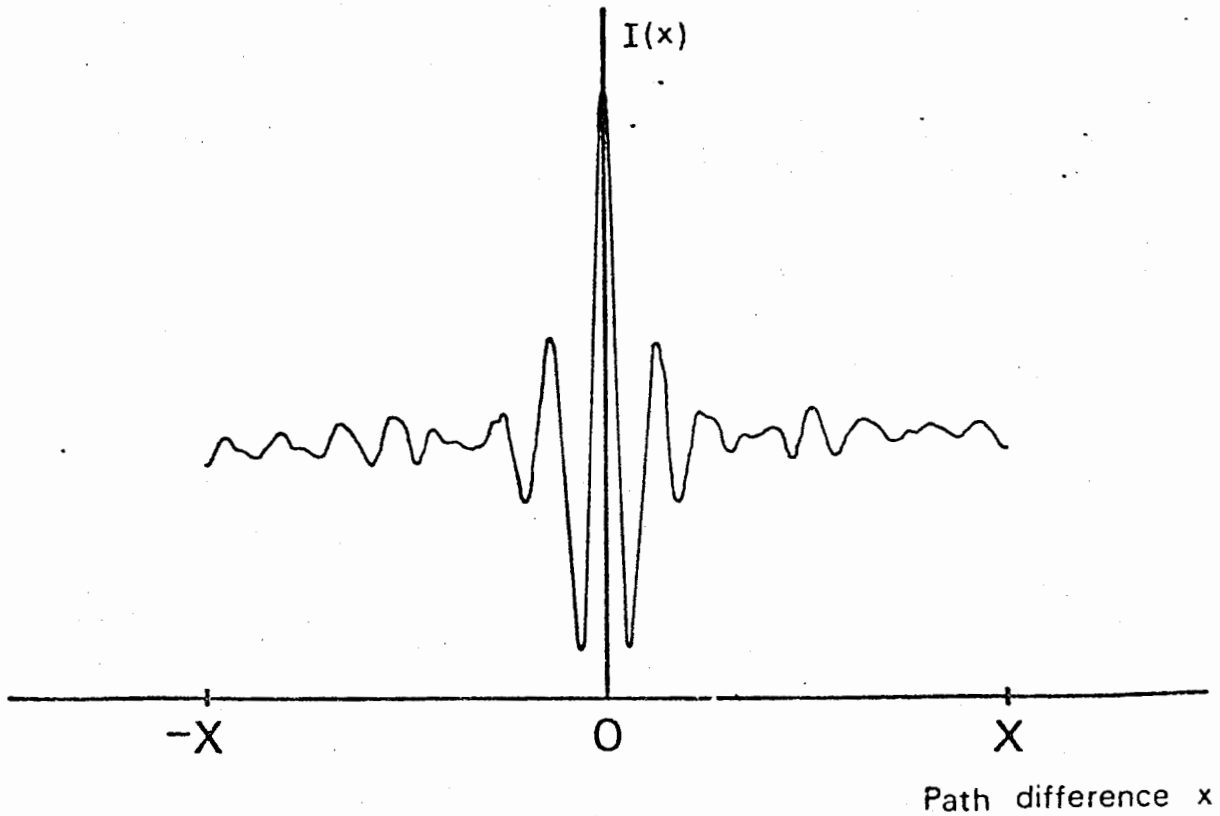

Fig. 2.2

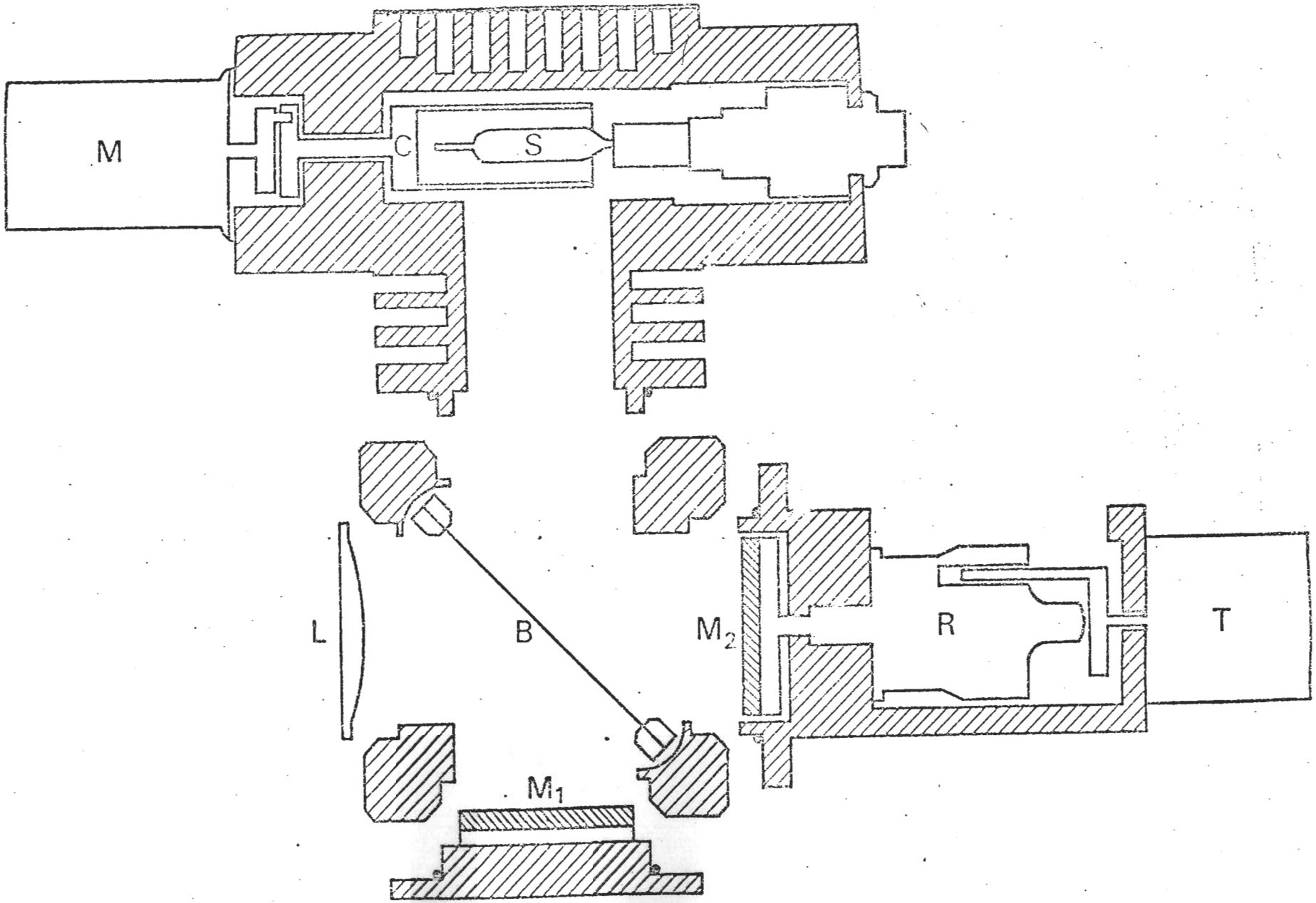

Fig. 2.3

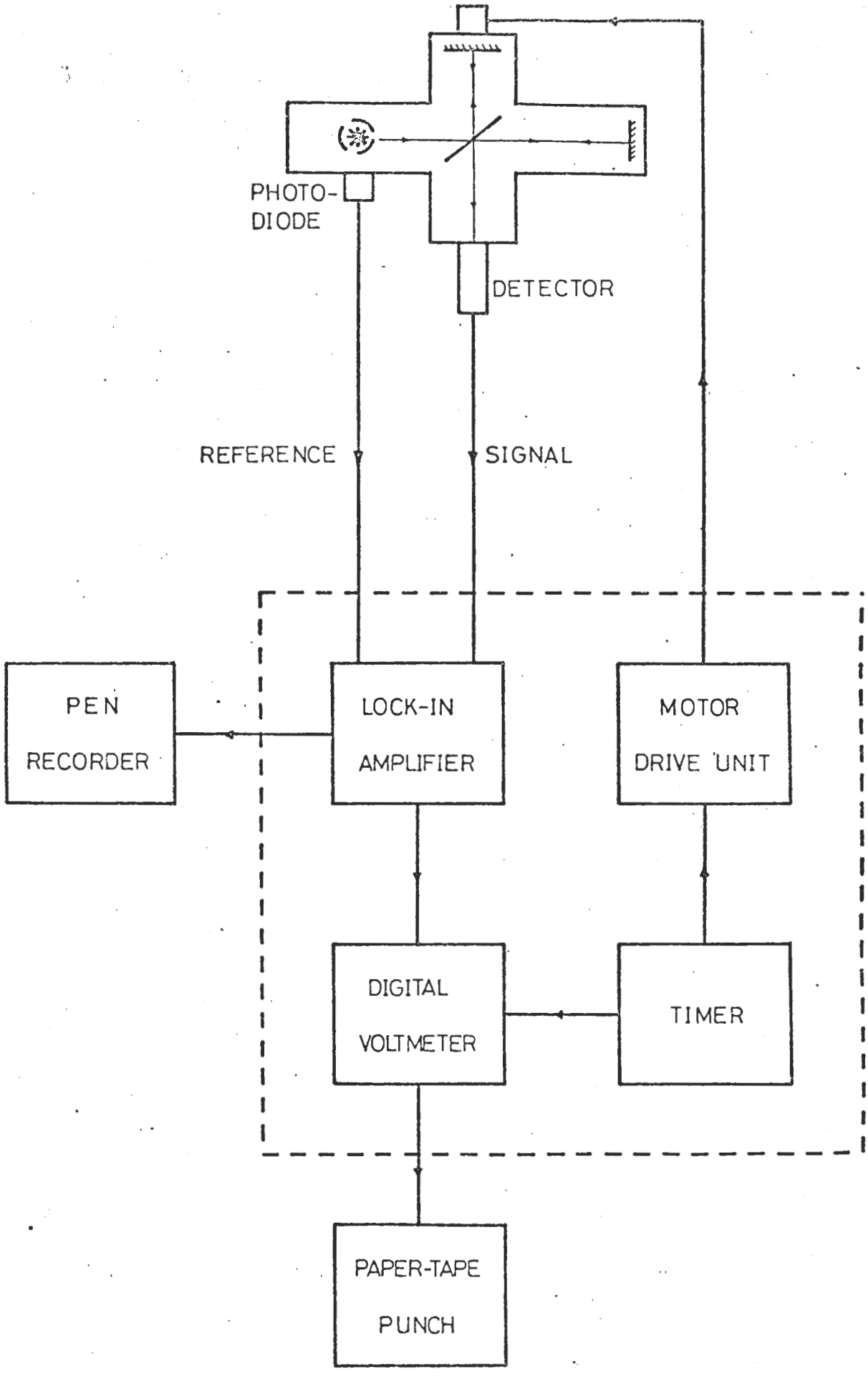
PHOTO-
DIODE
DETECTOR
REFERENCE
SIGNAL
PEN
RECORDER
LOCK-IN
AMPLIFIER
MOTOR
DRIVE UNIT
DIGITAL
VOLTMETER
TIMER
PAPER-TAPE
PUNCH

Fig. 2.4

Fig. 2.5

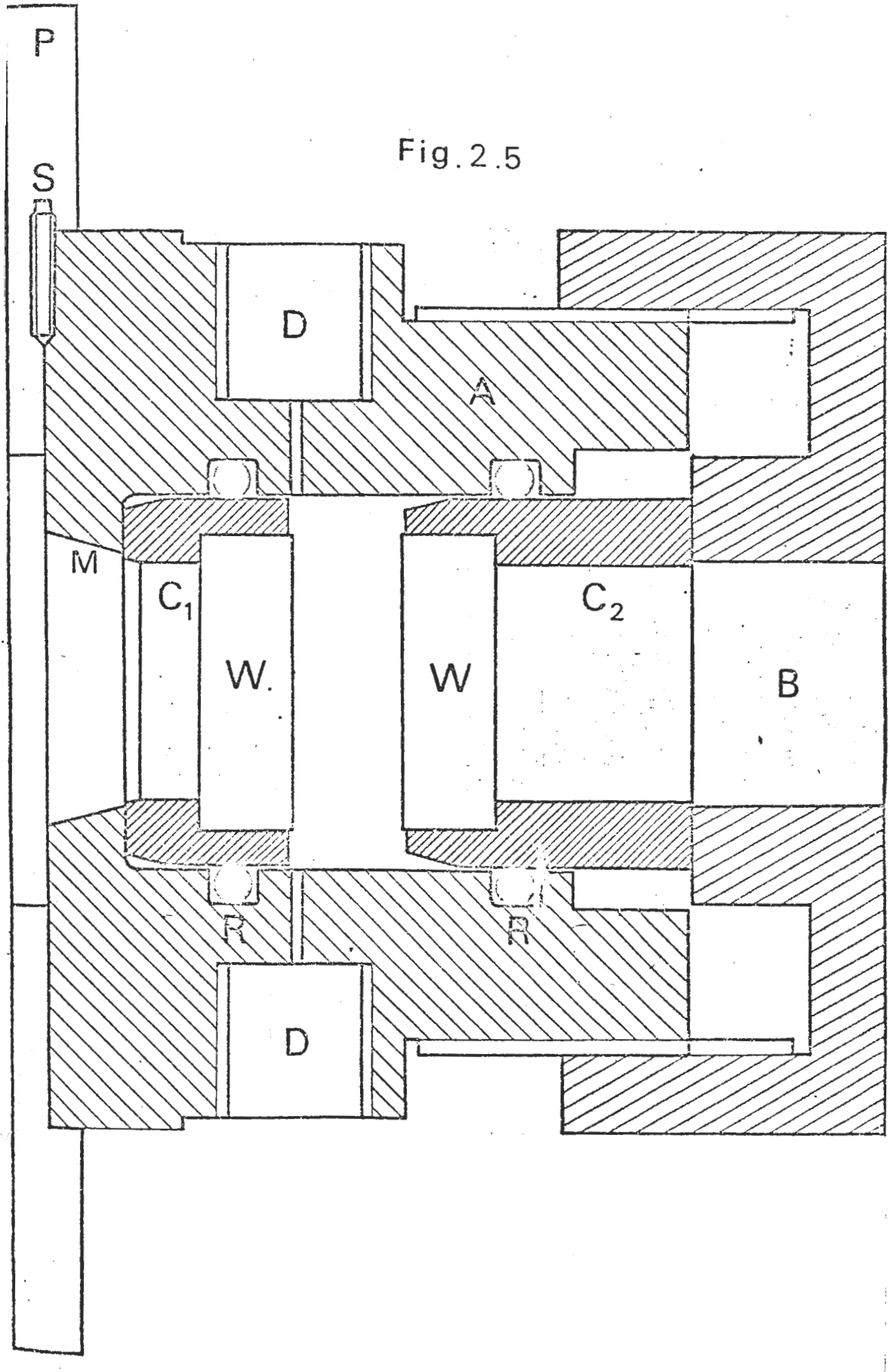

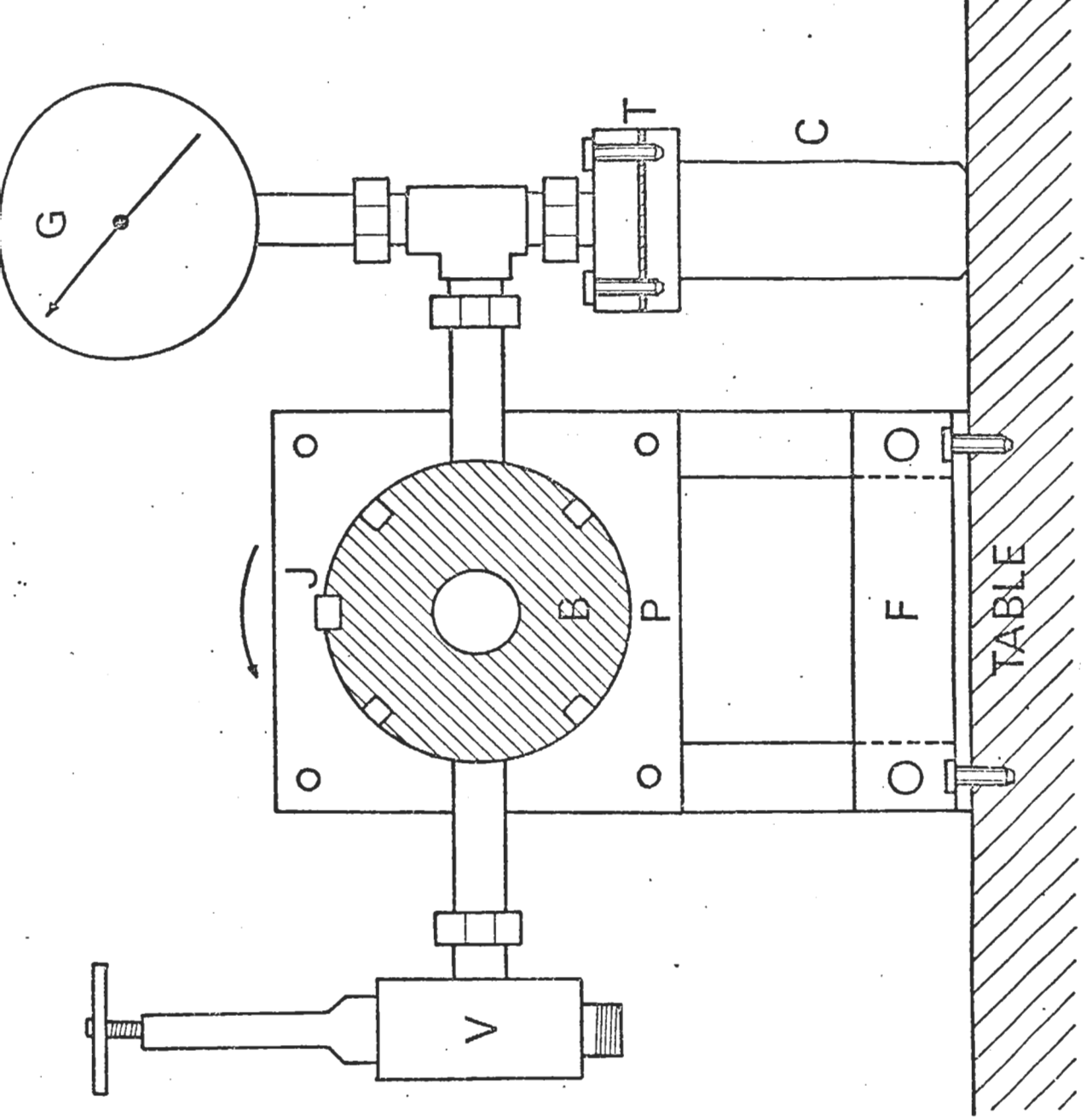

Fig. 2.6

$$\hat{S}_p(j\Delta\bar{\nu}) = \frac{1}{F} \cdot \sum_{k=0}^{2N-1} F_p(k\Delta x)\exp(-i(\pi/N)jk), \qquad (38)$$

$j = 0, 1, \ldots .(N-1)$. This is now in discrete Fourier transform form, ready for computation.

In practice, we cannot construct $F_p(x)$, since we need to know $F(x)$ for all x. Therefore $F(x)$ is truncated at $\pm X$, introducing the loss of resolution; $P(\bar{\nu})$ now being the "real" $P(\bar{\nu})$ convolved with a spectral window. Δx is then chosen to avoid aliasing, thereby fixing the cut-off wavenumber, $F = 1/\Delta x$ The truncated $F(x)$ is taken as one period of a periodic function, so that $F_p(x) = F(x)$ in the interval $[-X, X]$. The number of points $2N$ is fixed by the choice of X and Δx, since, from (37), $N = X/\Delta x$. From (38) we calculate N points of the complex spectrum $\hat{S}_p(\bar{\nu})$, which is $\hat{S}(\bar{\nu})$ if we avoid aliasing.

Finally, if we multiply the interferogram $F(x) = F_p(x)$ by a weighting function $W(x) = G(x)\cos^2(\pi x/2X)$, then (38) becomes:

$$\hat{S}(j\Delta\bar{\nu}) = \frac{1}{F} \sum_{k=0}^{2N-1} W(k\Delta x)F(k\Delta x)\exp(-i(\pi/N)jk) \qquad (39)$$

$j = 0, 1, \ldots,(N-1)$.

This was computed on an Elliot 4130 using a fast Fourier transform programme adopted by Baise (45).

The N.P.L/Grubb-Parsons Cube Interferometer

The optical components are shown in fig. 2.3, and the electronic in fig. 2.4. The source (S) is a high-pressure mercury-vapour lamp run off a choked mains supply, the radiation from the hot quartz

envelope being exceeded by black body emission from the plasma of the lamp below 100 cm^{-1}. The lamp is fan cooled. The beam-divider (B) is a stretched film of poly(ethylene terephthalate). Internal reflection in the film determines the transmission characteristics of the instrument. It can be shown that using a beam-divider, thickness t and refractive index n, the overall transmission of the interferometer will be a minimum at frequencies defined by:

$$\bar{\nu}_{min} = m / (2t(n^2 - \sin^2\theta))$$

where m is an integer, and θ is the angle of incidence of the radiation on the beam divider (usually 45°). Therefore, various thicknesses of beam dividers have to be used for different spectral ranges (39).

The detector used was a Golay pneumatic detector (47, 48) with a quartz window. Radiation above 400 cm^{-1} was cut off with a black poly(ethylene) filter. The detector was found to be reliable down to 15 cm^{-1} with averaging of repeated measurements. The reference signal was taken from the synchronous modulator motor (M) and was fed, together with the signal from the Golay detector to the lock-in amplifier. The d.c. signals of the sampled interferograms functions were displayed on the digital voltmeter, and recorded on paper tape at second intervals in binary coded decimal.

Channel Spectra

These are spurious peaks sometimes arising on the absorption spectrum from multiple internal reflections occurring somewhere in the radiation path, and they appear as a sine wave superimposed on the spectrum. Consider a plane parallel "plate" of thickness d,

which may be a solid window or a gaseous/liquid sample contained between two windows. Multiple internal reflections can occur within the plate. For almost normal incidence, the emerging beam will interfere constructively when their optical path difference 2nd is an integral multiple of any wavelength λ in the beam:

$$2nd = m\lambda$$

where n is the refractive index of the material, and m is an integer. The wavenumber difference between two successive maxima (or minima) is then $\Delta\bar{\nu} = 1/2nd$ with the first maximum at $\Delta\bar{\nu}$. Slight wedging of the ''window'' can reduce the channel spectra, although the wedged plates tend to act as prisms, and the thickness d becomes uncertain, which is limiting on the uncertainty in $\alpha(\bar{\nu})$ for small d.

Absorption Cells

For gas work, a variable path-length high pressure cell, designed by Baise and Horzelski (45) was used. The cell is shown in figs. 2.5 and 2.6. It allows a continuous change of sample thickness without releasing the pressure, and has 7mm Z-cut crystalline quartz windows, thus restricting the spectral range to below 130 cm^{-1}. Rotation through 18° corresponds to a change in sample thickness of 0.11 mm, the maximum sample thickness obtainable being 13.9 mm. The cell is placed in the atmosphere, the radiation entering (B) as a converging beam from the poly(ethylene) lens in the interferometer. B is a brass nut, and plate P is bolted to the support F which is secured to the bench. V is an Ermeto stainless-steel high-pressure, fine control needle valve, and G is a Budenberg pressure gauge. C is a stainless-steel drying chamber sealed with the gasket T containing

pre-baked type 3A zeolite drying agent.

A liquid in equilibrium with its vapour could be studied by rotating the whole cell in the direction of the arrow (fig. 2.6) so that liquid from C ran between the windows. Excepting gaseous cyanogen, both vapour and liquid spectra were obtained by comparing two thicknesses d_1 and d_2 ($d_2 > d_1$) so that:

$$\alpha(\bar{\nu}) = \frac{1}{(d_2 - d_1)} \cdot g_r \cdot \log_e \frac{I_0(\bar{\nu})}{I(\bar{\nu})}$$

The cells used with the work on MBBA were of two types. The first was a variable path-length VC-01 commercially available R.I.I.C. produced one with a maximum path length of 5.5 mm. Windows were of quartz, poly(propylene), or poly(4-methyl pent-1-ene) depending on spectral and chemical factors. The second was a fixed path length R.I.I.C. F - Cl cell modified for use with high fields transverse to the optical axis (see below).

Purification Techniques and Experimental Conditions

Gases

The gaseous spectra were obtained by taking the ratio of the mean of a number of sample interferograms to the mean of several background (1 atm dry air) interferograms in the case of cyanogen, using various path lengths up to the maximum available of 13.9 mm.

Cyanogen

The nominal purity of the commercial sample (Matheson) used was 98.6% w/w min., having the following specified impurities, whose dipole moments are appended: HCN (0.1 %, 2.98 D); CO_2(0.5 %, 0D)

Cl_2 (0.1%, 0D); CNCl (0.8%, 2.82D); H_2O (0.0%, 1.85D); N_2(trace, 0D); HCl (0.0%, 1.08D). The HCN could be removed by passage through $AgNO_3$ solution, and the CNCl frozen out in glass spirals immersed in a CO_2(s)/acetone bath at 258K, which also acted as preliminary removers of moisture. The gas was then passed through drying towers of pre-baked type 3A zeolite, (these were later replaced by a column cooled to about 260K with a jacket of CO_2(s)/propan-2-ol), and was condensed in a dried and nitrogen-filled cold-finger condenser, protected from atmospheric moisture by a drying tube of the same zeolite.

The cell was prepared by first purging repeatedly with dry nitrogen up to 50 bar; followed by evacuation to a few m bar, together with heating to 373K in order to remove all adsorbed moisture. The heating and evacuation were continued for 24 h before admission of the purified material. This was carried out by distillation from the cold finger condenser onto a large amount of dry zeolite contained in the cell sample chamber, which was immersed in a CO_2(s)/acetone bath at 247 $\pm$ K.

A sample of gas taken from the cell showed no trace of CNCl by mass spectrometric analysis. Moisture analysis on a similar sample, using a microtitration technique with Karl-Fischer reagent (at B.P. Chemicals (Int.) Ltd., Baglan Bay) revealed a content of 0.05 % w/w: this would contribute only very slightly to the measured absorption (13). Any significant absorption by polar molecule contamination would itself provide a contribution linearly dependent on the total pressure: the departures from the experimental pressure squared dependence were too small to provide any evidence of this.

Pressures of up to 33.5 $\pm$ 0.3 bar were obtained by heating

the liquid in the drying chamber of the cell up to 373K, the absorption cell being maintained at least 10K higher with electric heating tape and asbestos shielding to prevent condensation of cyanogen on the inside of the windows. It was implicit in the method of obtaining the vapour spectra that at each different pressure a new sample of vapour was used, thus giving a check on the efficiency of the purification technique, judging from the reproducibility of the liquid spectra.

The scatter due to noise, (electronic, mechanical, and heat effects on the Golay detector) in individual runs caused an uncertainty (about the plotted mean of many interferogram ratios) of at most 10% in the value of each A.(chapter 1); one of the sources of uncertainty is in the extrapolation to $\tilde{\nu} = 0$ from $\tilde{\nu} = 20$ cm^{-1}. The uncertainty in N arise in part from the temperature gradient between the front and back windows of the cell, which produces an uncertainty of $\pm$ 1.5% on the mean Kelvin temperature. The pressure, as monitored by a Budenberg gauge, was constant to $\pm$ 0.3 bar once equilibrium of the cell heating systems was obtained (ca. 4h). Another uncertainty arises from the difference in the values of N as obtained from generalised compressibility factors (49) and the Berthelot equation (ca. 2%). All these factors provide a total uncertainty in N of $\pm$ 3.5%. The density of the liquid was estimated from the relation (50)

$\rho = 0.91506\ (1 - 0.00203T)$ (T in ^{o}C; units: gm cm^{-3}).

Propyne

Pressures of up to 25.3 bar in the gas were obtained by heating the liquid in the drying chamber of the cell up to 376K. All individual spectra in this case were obtained by ratioing three transformed interferograms at a long path length to three at a shorter

path length. For the liquid, this eliminates effects arising from refractive index changes inherent in ratioing sample to background (51). The nominal purity (Matheson) was 96.0 mole % (min.), a typical analysis being: propyne (97.9 mole %), ethyne (0.1 mole %); dimethyl ether (1.2 mole %); dimethyl ethyne (0.1 mole %), allene (0.5 mole %); unidentified impurities, including moisture (0.2 mole %). Moisture content was minimised by passing the gas through a drying tower containing freshly baked 3A zeolite. The dried stream was then condensed over the same zeolite at about 243K in a vessel protected from atmospheric moisture. The condensate was then distilled into the drying chamber of the cell. Dimethyl ether is the other polar impurity present in any significant amounts: as the integrated absorption will be, to a good approximation, in the ratio of the $N\mu^2$ terms, we can estimate that the presence of 1.2 mole % of dimethyl ether will increase the absorption by 2.1 % above the value to be found were it replaced by propyne.

Propyne/CCl_4 solutions were prepared by bubbling the dried gas into spectroscopic grade carbon tetrachloride over type 3A zeolite, and thence through a drying tube outlet. M(propyne) in carbon tetrachloride was estimated immediately before, during, and after the six interferometric runs using the reaction:

$$2H\text{-}C\equiv C-Me + K_2HgI_4 + 2KOH \rightarrow (Me-C=C-)_2 Hg\downarrow + 4KI + 2H_2O$$

An excess of 0.5M solution of the alkali was added to the sample containing the mercury complex (0.979 mmole) and titrated immediately with 0.25M sulphuric acid. Three analyses gave the accepted (mean) concentration. Losses by outgassing of propyne during the time

needed to complete six interferograms were negligible. The VC - 01 cell was hermetically sealed as a further precaution.

The scatter due to noise in individual values of $\alpha(\tilde{\nu})$ was estimated by taking the standard deviation of several (up to eighteen) computations. This, together with uncertainties due to extrapolation to $\alpha(\tilde{\nu}) = 0$ at high and low $\tilde{\nu}$ gives an uncertainty in A of about $\pm$ 10%. The uncertainty in N arises from the temperature gradient, as for cyanogen; the uncertainty ($\pm$ 0.3 bar) in reading the Budenberg gauge; and from the difference in N as predicted by the Dieterici equation of state and generalised compressibility curves. The overall uncertainty in N is about $\pm$ 3% in the compressed gas.

The densities of liquid propyne at the three temperatures studied were estimated using a rectilinear diameters plot (52) with the equation (53):

$$\log_{10} P(\text{torr}) = 7.7514 - 1230.7/K \quad (K = \text{temp in K}),$$

to estimate the vapour pressure curve up to the critical point (402.39K, 55.54 $\pm$ 0.02 bar). Literature (54, 55) values of liquid propyne densities up to 273K were used in this estimation.

Nematogenic and Isotropic MBBA

For pure MBBA, the VC - 01 variable path length cell was used for measurements at room temperature and higher, best discrimination on $\alpha(\tilde{\nu})$ being obtained by a sample path length difference of 0.16mm. Direct comparison of $\alpha(\tilde{\nu})$ with and without the presence of a d.c. field was obtained using a variety of very simple fixed path length cells, based on the F - 01, using wire (0.075 mm o.d.) electrodes between two spacers. No attempt was made to obtain a uniformly oriented

sample of the mesophase by pretreatment of the surfaces of the cell.

The spectra, for samples above room temperature, were taken in an electrically heated VC - 01 cell, the fluctuations in temperature (read from a calibrated copper-constantan thermocouple) being typically $\pm$ 2K. Judged from the sharpness of the nematic - isotropic transition at 320K, the MBBA sample used (from Eastmann-Kodak) was of an acceptable purity. It was kept dry under nitrogen at 273K by standing over type 3A zeolite when not in use. To check on decomposition, several interferograms were run (for up to 3h) in the isotropic phase at 358K, then the cell was cooled and several further spectra recorded at 296K. The latter $\alpha(\tilde{\nu})$ values agreed within $\pm$ 5% with those obtained from fresh, pure, unheated samples. Thin layer chromatography could detect no difference between these latter and samples held at 358K for 3h. Solutions were made up by weight in pure, dry solvents.

The mean $\alpha(\tilde{\nu})$ values presented have an uncertainty of $\pm$ 5% or less except at > 170 cm^{-1}, due to beam divider characteristics, and occasionally at 130 ± 5 cm^{-1} owing to the intensity of the peak absorptions there. All accepted spectra were the weighted means of at least three sample runs, usually at each of two thicknesses, ratioed against three background runs. Evaluations of A involved extrapolation of the observed $\alpha(\tilde{\nu})$ at both high and low values. With the aid of microwave measurements (56, 57) the extrapolation to $\tilde{\nu} = 0$ leaves relatively little uncertainty, but at $\tilde{\nu} > 170$ cm^{-1} the absorption centred near 130 cm^{-1} is overlapped by a neighbouring feature: the contribution of the latter has been estimated to result in an uncertainty of $\pm$ 10% in the integrated intensity being determined.

CHAPTER 3

Equations for Bimolecular Collision-induced Absorption in Symmetric Top and Linear Molecules.

The general theory of pressure induced absorption by symmetric top molecules has been recently given by Frost (58). The purpose of this chapter is to use this theory to derive equations for multipole-induced dipolar absorption in symmetric top and linear molecules in forms suitable for digital computation. Some of the resulting equations are then used to interpret the far infra-red absorption spectrum of compressed gaseous oxygen (7).

The dipole induced in a molecule by the field of another in a bimolecular collision can be evaluated using Frost's treatment by expanding the field in terms of point multipoles, assuming the following.

(i) An eigenstate of the interacting pair is taken as the product of the eigenstates of the isolated molecule. This is adequately correct only for a purely central intermolecular force field U(R), which can then be approximated by a Lennard-Jones potential.

(ii) The centre-of-mass motion of each molecule in a pairwise interaction is treated classically, with each molecule at rest, so translational absorption is ignored.

The basic equation for the intensity of the bimolecular collision induced absorption is as follows:

$$I_{AA} = \frac{4\pi^3 \bar{\nu} N^2}{3hc} \sum_{\substack{i,f \\ E_f - E_i = h\nu}} \left(\frac{F_i^{AA}}{d_i^{AA}} - \frac{F_f^{AA}}{d_f^{AA}} \right) \int_0^\infty 4\pi R^2 \exp(-U_{AA}(R)/kT)$$

$$\times \sum_{m_i, m_f} \left| \langle i m_i | \underline{\mu}^{AA}(R) | f m_f \rangle \right|^2 dR \qquad (1)$$

where $\underline{\mu}(R)$ is the induced dipole moment of a pair of molecules separated by a distance R, and where $|im_i\rangle$, $|fm_f\rangle$ denote in general rotation-vibration eigenstates for the pair, with m_i, m_f as degenerate magnetic quantum numbers. The summations over the quantum numbers i,f are restricted to those transitions $i \rightarrow f$ for which the absorbed frequency $\left[h^{-1}(E_f - E_i)\right]$ lies in the absorption band of (approximate) frequency ν. The quantities d_i, d_f are the degeneracies of the quantum numbers i,f respectively. $U_{AA}(R)$ is the intermolecular potential energy. F_i is given by the Maxwell-Boltzmann expression:

$$F_i = d_i \exp(-E_i/kT)/Z \qquad (2)$$

where the partition function $Z = \sum_i d_i \exp(-E_i/kT)$ (3)

the summation being carried out over all allowed energy levels. Hence it can be shown that:

$$\sum_{\substack{i,f \\ E_f - E_i \doteq h\nu}} \left(\frac{F_i^{AA}}{d_i^{AA}} - \frac{F_f^{AA}}{d_f^{AA}} \right) = \frac{1}{Z} \exp(-E_i/kT)(1-\exp(-hc\,\bar{\nu}_{if}/kT)) \qquad (4)$$

The matrix elements $\sum |\langle im_i | \underline{\mu}^{AA}(R) | fm_f \rangle|^2$ are expanded by Frost (his equation 24) as:

$$\sum_{\lambda_1, \lambda_2} \left(\sum |Fm|^2 \right) \frac{(2J_1+1)}{2\lambda_1+1} . C(J_1, \lambda_1, J_1'; K_1, K_1' - K_1, K_1')^2$$

$$\times \frac{(2J_2+1)}{2\lambda_2+1} C(J_2, \lambda_2, J_2'; K_2, K_2' - K_2, K_2')^2 \qquad (5)$$

where $\sum |Fm|^2$ is listed in Table 3.1 for various λ_1 and λ_2. The C( ) denote some relevant Clebsch-Gordan coefficients. In Table 3.1, μ, Q, Ω, and Φ denote the permanent dipole, quadrupole, octupole and hexadecapole moments respectively of each molecule. $\alpha_o = \frac{1}{3}(\alpha_{//} + 2\alpha_\perp)$ is the mean molecular polarisability, and $\delta = (\alpha_{//} - \alpha_\perp)$ is the anisotropy of polarisability.

Symmetric Top Molecules

Selection Rules in the Summation (5)

1) One of λ_1 or λ_2 must be 0 or 2.

2) Any ΔJ_1, ΔJ_2 is allowed, provided one of $|\Delta J_1|$, $|\Delta J_2| \leqslant 2$. $\Delta K_1 = \pm m_1 n_1$, $\Delta K_2 = \pm m_2 n_2$, provided one of m_1, $m_2 = 0$; $m_1 = 0$ if $|\Delta J_2| > 2$, $m_2 = 0$ if $|\Delta J_1| > 2$. Here, m_1 or m_2 is a positive integer, or zero, while n_1 or n_2 denotes the rotational symmetry class of molecule 1 or molecule 2 respectively. For symmetric tops, $n_1 = n_2 = 3$.

3) If $K_1 = K_1' = 0$; $K_2 = K_2' = 0$, then $\lambda_1 + \Delta J_1$, and $\lambda_2 + \Delta J_2$ must be even for contribution.

The allowed transitions, neglecting multipole terms greater than the octupole, are ticked in Table 3.2, together with the corresponding (λ_1, λ_2) factors allowed by the selection rules, and by general limitations on Clebsch-Gordan coefficients (59). Summing the different (λ_1, λ_2) factors gives the relevant Clebsch-Gordan coefficients to be used in equation (5), and these are shown in Table 3.3. For convenience, the summation (5) can be split into the dipole-induced dipole (R^{-6}), quadrupole-induced dipole (R^{-8}) and octupole-induced dipole terms:

Table 1.

The Coefficients $\sum |Fm|^2$ for various (λ_1, λ_2)

λ_1	λ_2	$\sum \|Fm\|^2$
0	1	$6\,\alpha_0^2 \mu^2\, R^{-6}$
0	2	$15\,\alpha_0^2\, Q^2\, R^{-8}$
1	2	$\frac{20}{3}\,\delta^2 \mu^2\, R^{-6}$
2	2	$\frac{40}{3}\,\delta^2\, Q^2\, R^{-8}$
0	3	$28\,\alpha_0^2\, \Omega^2\, R^{-10}$
2	3	$\frac{280}{9}\,\delta^2\, \Omega^2\, R^{-10}$
0	4	$45\,\alpha_0^2\, \Phi^2\, R^{-12}$
2	4	$\frac{150}{3}\,\delta^2\, \Phi^2\, R^{-12}$

Allowed Transitions up to the Octupole Moment Term in Symmetric Tops (✓)

ΔJ_1	ΔJ_2	ΔK_1	ΔK_2	(λ_1, λ_2)										
				(0,3)	(0,2)	(0,1)	(1,2)	(1,0)	(2,3)	(2,2)	(2,1)	(2,0)	(3,2)	(3,0)
0	1	0	0	✓	✓	✓	✓	X	✓	✓	✓	X	✓	X
0	2	0	0	✓	✓	X	✓	X	✓	✓	X	X	✓	X
1	0	0	0	X	X	X	✓	✓	✓	✓	✓	✓	✓	✓
1	1	0	0	X	X	X	✓	X	✓	✓	✓	X	✓	X
1	2	0	0	X	X	X	✓	X	✓	✓	X	X	✓	X
2	0	0	0	X	X	X	X	X	✓	✓	✓	✓	✓	✓
2	1	0	0	X	X	X	X	X	✓	✓	✓	X	✓	X
2	2	0	0	X	X	X	X	X	✓	✓	X	X	✓	X
3	0	0	0	X	X	X	X	X	X	X	X	X	✓	✓
3	1	0	0	X	X	X	X	X	X	X	X	X	✓	X
3	2	0	0	X	X	X	X	X	X	X	X	X	✓	X
0	3	0	0	✓	X	X	X	X	✓	X	X	X	X	X
1	3	0	0	X	X	X	X	X	✓	X	X	X	X	X
2	3	0	0	X	X	X	X	X	✓	X	X	X	X	X
3	0	3	0	X	X	X	X	X	X	X	X	X	✓	✓
3	1	3	0	X	X	X	X	X	X	X	X	X	✓	X
3	2	3	0	X	X	X	X	X	X	X	X	X	✓	X
0	3	0	3	✓	X	X	X	X	✓	X	X	X	X	X
1	3	0	3	X	X	X	X	X	✓	X	X	X	X	X
2	3	0	3	X	X	X	X	X	✓	X	X	X	X	X

Table 3.3

Glebsch-Gordan Coefficients to be used up to the Octupole Term in Equation (5.13)

(λ_1, λ_2)	No. of Times	Clebsch-Gordan Coefficients	Term
(1,0) or (0,1)	2	$C(J,1,J';\ K,0,K')^2 C(J,0,J';\ K,0,K')^2$	Dipole
(2,0) or (0,2)	4	$C(J,2,J';\ K,0,K')^2 C(J,0,J';\ K,0,K')^2$	Quadrupole
(2,2)	8	$C(J,2,J';\ K,0,K')^2 C(J,2,J';\ K,0,K')^2$	Quadrupole
(2,1) or (1,2)	10	$C(J,2,J';\ K,0,K')^2 C(J,1,J';\ K,0,K')^2$	Dipole
(3,0) or (0,3)	6	$C(J,3,J';\ K,0,K')^2 C(J,0,J';\ K,0,K')^2$	Octupole
	2	$C(J,3,J';\ K,3,K')^2 C(J,0,J';\ K,0,K')^2$	
(3,2) or (2,3)	22	$C(J,3,J';\ K,0,K')^2 C(J,2,J';\ K,0,K')^2$	Octupole
	6	$C(J,3,J';\ K,3,K')^2 C(J,2,J';\ K,0,K')^2$	

Dipole-Induced Dipole Intensity

The intensity of a single dipole-induced ($J \rightarrow J + 1$) transition resulting from the bimolecular collision of symmetric top molecules is given from equation (5) and Table 3.3 as:

$$A^{\mu}_{J\rightarrow J+1} = \frac{4\pi^3 \mu^2 N^2}{3hc\ Z} \int_0^{\infty} 4\pi^2 R^{-4} \exp(-U_{AA}(R)/kT)dR$$

$$x \sum_{K=-J}^{J} \left[(1-\exp(hc\,\bar{\nu}_1(J)/kT))\exp(-E_{JK}\,hc/kT)\,\bar{\nu}_1(J) \right.$$

$$\left. x\ (4\alpha_o^2 f_1(J,K) + \frac{40}{3}\ \frac{\delta^2 f_1^2(J,K)K^2)}{J(J+2)} \right] \qquad (6)$$

where $\bar{\nu}_1(J) = 2B(J+1)$, $f_1 = (J-K+1)(J+K+1)/(J+1)$.

In this equation, $E_{JK} = BJ(J+1) + (A-B)K^2$, where A and B are the rotational constants of a symmetric top molecule. The quantum numbers J and K can be defined through the facts that the total angular momentum is equal to $(h/2\pi)\sqrt{(J(J+1))}$, and that the component of angular momentum along the symmetry axis is equal to $(h/2\pi)K$.

Quadrupole-Induced Dipole Intensity

Similarly, from (5) and Table 3.3:

$$A^{Q}_{J\rightarrow J+2} = \frac{4\pi^3 Q^2 N^2}{3hcZ} \int_0^{\infty} 4\pi^2 R^{-6} \exp(-U_{AA}(R)/kT)dR$$

$$x \sum_{K=-J}^{J} \left[(1-\exp(-hc\,\bar{\nu}_2(J)/kT))\exp(-E_{JK}hc/kT)\,\bar{\nu}_2(J) \right.$$

$$\left. x\left(18\alpha_o^2 f_2(J,K) + \frac{48}{5}\ \delta^2 f_2^2(J,K)\right) \right] \qquad (7)$$

where $\bar{\nu}_2(J) = 2B(2J + 3)$

$$f_2(J,K) = \frac{(J-K+2)(J-K+1)(J+K+2)(J+K+1)}{(J+1)(J+2)(2J+3)}$$

Octupole-Induced Dipole Intensity

From (5) and Table 3.3:

$$A^{\Omega}_{J\to J+3} = \frac{4\pi^3\Omega^2 N^2}{3hc\ Z}\int_0^{\infty} 4\pi^2 R^{-8}\exp(-U_{AA}(R)/kT)dR$$

$$x \sum_{K=-J}^{J}\left[(1-\exp(-hc\bar{\nu}_3(J)/kT))\exp(-E_{JK}hc/kT)\bar{\nu}_3(J)\right.$$

$$\left. x\ ((24x' + 8y)\alpha_o^2 + (176x'/9 + 16y/3)_w\delta^2)\right] \qquad (8)$$

where

$$x' = \frac{5(J+K+3)(J+K+2)(J+K+1)(J-K+3)(J-K+2)(J-K+1)}{(J+2)(J+3)(2J+2)(2J+3)(2J+5)}$$

$$y = \frac{(J+K+3)(J+K+2)(J+K+1)(J-K+3)(J-K+2)(J-K+1)}{(2J+2)(2J+3)(2J+4)(2J+5)(2J+6)}$$

$$w = \frac{3(J-K+2)(J-K+1)(J+K+1)(J+K+2)}{(2J+2)(2J+3)(J+2)}$$

$$\bar{\nu}_3(J) = 6B(J+2)$$

Linear Molecules

Selection Rules

1) $K_1 = K_1' = K_2 = K_2' = 0$

2) One of λ_1 or λ_2 must be 0 or 2.

3) $\lambda_1 + \Delta J_1$ and $\lambda_2 + \Delta J_2$ must be even.

4) $\lambda_1 \geqslant |\Delta J_1|$; $\lambda_2 \geqslant |\Delta J_2|$.

The allowed ΔJ_1 and ΔJ_2 are restricted by what are taken to be the important multipole moments. If the hexadecapole (Φ) is the last important moment, the summation in (5) is over $\lambda_1 \leqslant 4$, $\lambda_2 \leqslant 4$. In this case, the allowed ΔJ_1, ΔJ_2 transitions, and the associated allowed (λ_1, λ_2) factors, are shown in Table 3.4. The number and type of Clebsch-Gordan coefficients thus contributing to (5) are shown in Table 3.5. Using this table with equation (5), then the equation for the various multipole-induced dipole absorption intensities in linear molecules come out as below:

Dipole-Induced Dipole Absorption

$$\alpha^{A}_{J\to J+1} = \frac{4\pi^3 \mu^2 N^2}{3hc\, Z} \int_0^\infty 4\pi^2 R^{-4} \exp(-U_{AA}(R)/kT)\, dR$$

$$\times \left(1-\exp(-hc\, \bar{\nu}_1'(J)/kT)\right) \exp(-E_J hc/kT)\, \bar{\nu}_1'(J)$$

$$\times \left(4\alpha_0^2 (J+1) + \frac{8}{3} \delta^2 \frac{(J+1)^2(J+2)}{(2J+3)}\right) \qquad (9)$$

with $E(J) = BJ(J+1)$, $\bar{\nu}_1'(J) = 2B(J+1)$.

Table 3.4

Allowed (λ_1, λ_2) up to the Hexadecapole term in Linear Molecules. (✓).

J_1	J_2	(λ_1, λ_2)														
		(0,1)	(1,0)	(2,1)	(2,2)	(0,2)	(2,0)	(1,2)	(3,0)	(3,2)	(0,3)	(2,3)	(4,0)	(4,2)	(2,4)	(0,4
1	0	X	✓	X	X	X	X	✓	✓	✓	X	X	X	X	X	X
0	1	✓	X	✓	X	X	X	X	X	X	✓	✓	X	X	X	X
2	0	X	X	X	✓	X	✓	X	X	X	X	X	✓	✓	✓	X
0	2	X	X	X	✓	✓	X	X	X	X	X	X	X	✓	✓	✓
1	1	X	X	X	X	X	X	X	X	X	X	X	X	X	X	X
2	1	X	X	✓	X	X	X	X	X	X	X	✓	X	X	X	X
1	2	X	X	X	X	X	X	✓	X	✓	X	X	X	X	X	X
2	2	X	X	X	✓	X	X	X	X	X	X	X	X	✓	✓	X
3	0	X	X	X	X	X	X	X	✓	✓	X	X	X	X	X	X
3	1	X	X	X	X	X	X	X	X	X	X	X	X	X	X	X
3	2	X	X	X	X	X	X	X	X	✓	X	X	X	X	X	X
3	3	X	X	X	X	X	X	X	X	X	X	X	X	X	X	X
0	3	X	X	X	X	X	X	X	X	X	✓	✓	X	X	X	X
1	3	X	X	X	X	X	X	X	X	X	X	X	X	X	X	X
2	3	X	X	X	X	X	X	X	X	X	X	✓	X	X	X	X
4	0	X	X	X	X	X	X	X	X	X	X	X	✓	✓	X	X
4	1	X	X	X	X	X	X	X	X	X	X	X	X	X	X	X
4	2	X	X	X	X	X	X	X	X	X	X	X	X	✓	X	X
4	3	X	X	X	X	X	X	X	X	X	X	X	X	X	X	X
4	4	X	X	X	X	X	X	X	X	X	X	X	X	X	X	X
3	4	X	X	X	X	X	X	X	X	X	X	X	X	X	X	X
2	4	X	X	X	X	X	X	X	X	X	X	X	X	X	✓	X
1	4	X	X	X	X	X	X	X	X	X	X	X	X	X	X	X
0	4	X	X	X	X	X	X	X	X	X	X	X	X	X	✓	✓

Table 3.5

Clebsch Gordan Coefficients summed from Table 3.4

(λ_1, λ_2)	No. of Times	C. - G. Coefficients	Term
(1, 0) or (0, 1)	2	$C(J,1,J';\ 0,0,0)^2 . C(J,0,J';\ 0,0,0)^2$	Dipole
(2,1) or (1,2)	4	$C(J,2,J';\ 0,0,0)^2 . C(J,1,J';\ 0,0,0)^2$	Dipole
(2,0) or (0,2)	2	$C(J,2,J';\ 0,0,0)^2 . C(J,0,J';\ 0,0,0)^2$	Quadrupole
(2,2)	3	$C(J,2,J';\ 0,0,0)^2 . C(J,2,J';\ 0,0,0)^2$	Quadrupole
(3,0) or (0,3)	4	$C(J,3,J';\ 0,0,0)^2 . C(J,0,J';\ 0,0,0)^2$	Octupole
(3,2) or (2,3)	8	$C(J,3,J';\ 0,0,0)^2 . C(J,2,J';\ 0,0,0)^2$	Octupole
(4,0) or (0,4)	4	$C(J,4,J';\ 0,0,0)^2 . C(J,0,J';\ 0,0,0)^2$	Hexadecapole
(4,2) or (2,4)	10	$C(J,4,J';\ 0,0,0)^2 . C(J,2,J';\ 0,0,0)^2$	Hexadecapole

Quadrupole-Induced Dipole Absorption

$$\ell^{A^{Q}}_{J\to J+2} = \frac{4\pi^3 Q^2 N^2}{3hc\ Z}\int_0^\infty 4\pi^2 R^{-6}\exp(-U_{AA}(R)/kT)dR$$

$$\times\ (1-\exp(-hc\bar{\nu}_2'(J)/kT))\exp(-E_J hc/kT)\bar{\nu}_2'(J)$$

$$\times\ (9\alpha_o^2\frac{(J+1)(J+2)}{(2J+3)} + \frac{18}{5}\delta^2\left(\frac{(J+1)(J+2)}{(2J+3)}\right)^2) \qquad (10)$$

where $\bar{\nu}_2'(J) = 2B(2J+3)$.

Octupole-Induced Dipole Absorption

$$\ell^{A^{\Omega}}_{J\to J+3} = \frac{4\pi^3 \Omega^2 N^2}{3hc\ Z}\int_0^\infty 4\pi^2 R^{-8}\exp(-U_{AA}(R)/kT)dR$$

$$\times\ (1-\exp(-hc\bar{\nu}_3'(J)/kT))\exp(-E_J hc/kT)\bar{\nu}_3'(J)$$

$$\times\ (40\alpha_o^2\frac{(J+1)(J+2)(J+3)}{(2J+3)(2J+5)} + \frac{80}{3}\delta^2\left(\frac{(J+1)(J+2)}{(2J+3)}\right)^2\frac{(J+3)}{(2J+5)}) \qquad (11)$$

where $\bar{\nu}_3'(J) = 6B(J+2)$.

Hexadecapole-Induced Dipole Absorption

$$\ell^{A^{\Phi}}_{J\to J+4} = \frac{4\pi^3 \Phi^2 N^2}{3hc\ Z}\int_0^\infty 4\pi^2 R^{-10}\exp(-U_{AA}(R)/kT)dR$$

$$\times\ (1-\exp(hc\bar{\nu}_4'(J)/kT))\exp(-E_J hc/kT)\bar{\nu}_4'(J)$$

$$\times\left(\frac{175}{2}\frac{(J+1)(J+2)(J+3)(J+4)}{(2J+3)(2J+5)(2J+7)}\alpha_o^2 + \frac{875}{12}\delta^2\left(\frac{(J+1)(J+2)}{2J+3}\right)^2\frac{(J+3)(J+4)}{(2J+5)(2J-}\right.$$

(12)

where $\nu_4'(J) = 4B(2J+5)$

In the above derivations, the Clebsch-Gordan coefficients not available in the literature (59) can be calculated from the general formula:

$$C(j_1,j_2,j;m_1,m_2,m) = \delta(m,m_1+m_2)\left[\frac{(j_1+j_2-j)!(j+j_1-j_2)!(j+j_2-j_1)!(2j+1)}{(j+j_1+j_2+1)!}\right]^{\frac{1}{2}}$$

$$\times \sum_k \frac{(-1)^k((j_1+m_1)!(j_1-m_1)!(j_2+m_2)!(j_2-m_2)!(j+m)!(j-m)!)^{\frac{1}{2}}}{k!(j_1+j_2-j-k)!(j_1-m_1-k)!(j_2+m_2-k)!(j-j_2+m_1+k)!(j-j_1-m_2+k)!}$$

where $\delta(i,j) = 0$ if $i = j$

$= 1$ if $i \neq j$.

Thus:

$$C(j_1,3,j;m_1,0,m) = \left[\frac{5(j_1+m+3)(j_1+m+2)(j_1+m+1)(j_1-m+3)(j_1-m+2)(j_1-m+1)}{(j_1+2)(j_1+3)(2j_1+1)(2j_1+2)(2j_1+3)(2j_1+5)}\right]^{\frac{1}{2}}$$

$$C(j_1,3,j;m_1,3,m) = \left[\frac{(j_1+m+3)(j_1+m+2)(j_1+m+1)(j_1-m+3)(j_1-m+2)(j_1-m+1)}{(2j_1+1)(2j_1+2)(2j_1+3)(2j_1+4)(2j_1+5)(2j_1+6)}\right]^{\frac{1}{2}}$$

$C(j_1,4,j;m_1,0,m) =$

$$\left[\frac{35(j_1+m+4)(j_1+m+3)(j_1+m+2)(j_1+m+1)(j_1-m+4)(j_1-m+3)(j_1-m+2)(j_1-m+1)}{8(2j_1+1)(j_1+1)(2j_1+3)(j_1+2)(2j_1+5)(j_1+3)(2j_1+7)(j_1+4)}\right]^{\frac{1}{2}} .$$

Application to the Case of Oxygen Gas

In this section, some of the above equations are used to simulate the observed (7) far infra-red (20 - 400) cm^{-1} spectrum of compressed gaseous oxygen. It is found that the overall experimental profile is reproduced fairly well by the use of profiles calculated on the basis of quadrupole and hexadecapole-induced dipolar absorption in the event of bimolecular collision. Values of $|Q|$ and $|\Phi|$ are obtained from the best fit to the experimental intensity and band shape. A justification for the use of the very short range (R^{-12} dependent) hexadecapole field is based on the evaluation of the approximate range of the corresponding field and its ability to induce a significant dipole.

The far infra-red spectrum (fig. 3.1) of compressed oxygen gas has been observed by Bosomworth and Gush (7) to be of exceptional breadth (160 cm^{-1} at half peak height). By comparison, the corresponding absorption (7) in nitrogen is much narrower, and is fairly well simulated by the frequencies and relative intensities of the unbroadened $\Delta J = 2$ rotational transitions calculated with an equation similar to (10). Bosomworth and Gush attributed the high frequency part of the oxygen spectrum to a short range overlap contribution to the dipole moment, but made no quantitative analysis of this phenomenon. However, with equations (10) and (12), it is possible to simulate the oxygen band with two contributions to the bimolecular collision induced dipole moments, assumed to arise from the quadrupole and hexadecapole moments of the field of the second oxygen molecule at the first and vice-versa. (Oxygen has no dipole or octupole moment by symmetry).

It is obvious that the hexadecapole field, being R^{-12} dependent, is important only at very short separations R. Justification for its use in the present case comes from a simple analysis given by Bosomworth and Gush involving a rough measurement of p, the range of the induced dipole moment, which may be obtained from the width of the spectrum. Classically, the spectrum is proportional to the Fourier transform of the autocorrelation function of the dipole moment, the width being inversely proportional to that of the autocorrelation function, which is roughly equal to the duration of the collision. Thus:

$$\tau = 1/(2\pi\bar{\nu}_{\frac{1}{2}}c)$$

where $\bar{\nu}_{\frac{1}{2}}$ is the width of the spectrum at half peak height. For oxygen at 300K, $\bar{\nu}_{\frac{1}{2}} = 160\ cm^{-1}$, thus $\tau = 1.0 \times 10^{-13}$ sec. Then p can be estimated by multiplying the duration of collision (τ) by the average rate of change of the intermolecular distance ($\dot{R}_{AV}$).

Now $\frac{1}{2}(m\dot{R}_{AV}^2) = \frac{1}{2}(kT)$, where m is the reduced mass of the colliding molecules. Thus $p = \dot{R}_{AV}\tau = 0.55\text{Å}$ at 300K. The Lennard-Jones diameter (σ) of an oxygen-oxygen pair is 7.92Å, thus the range of the induced dipole is about $\sigma/16$. The conclusion is the same as that of Bosomworth and Gush for neon-argon pairs - the induced dipole moment is essentially zero until the colliding O_2 molecules enter the repulsive region of the intermolecular potential, and rises rapidly as the molecules interpenetrate. Thus only collisions in which the impact diameter is less than σ contribute to the absorption, i.e. very short range fields such as the hexadecapole are expected, on this picture, to contribute significantly to the

dipole inducing process in that short interval of time when the two molecules are approaching and coming away from their point of greatest overlap.

Estimation of $|Q|$ and $|\Phi|$

Approximate values of $|Q|$ and $|\Phi|$ for oxygen can be estimated (fig. 3.1) by resolving the overall oxygen profile into a quadrupole-induced and hexadecapole-induced dipole absorption band. These are based on the line spectra calculated from the even J values in equations (10) and (12) (oxygen having no odd J contributions due to nuclear spin statistics). The considerable broadening of each line expected in practice might lead to a different overall profile from that suggested by the line spectrum alone; nevertheless, the agreement between the experimental and overall profiles is quite good, bearing in mind the experimental uncertainty.

By summing (10) and (12) over even J, and by comparison with the resolved areas, values of $|Q|$ and $|\Phi|$ can be determined for best fit. The integrals in (10) and (12) were evaluated using the tables of Buckingham and Pople (60) with Lennard-Jones parameters $\epsilon/k = 118K$, $\sigma = 3.46\text{Å}$. The other constants used are $B = 1.45\ cm^{-1}$, $\alpha_o = 1.60 \times 10^{-24} cm^3$, $\delta = 1.14 \times 10^{-24} cm^3$.

Thus $$\left(\sum_{2nJ} \rho A^{Q}_{J \to J+2} \right) = 3.61 \times 10^{-5} N^2 Q^2 \ cm^{-2}\ amagat^{-2} \qquad (13)$$

$$\left(\sum_{2nJ} \rho A^{\Phi}_{J \to J+4} \right) = 4.51 \times 10^{-5} N^2 \Phi^2 \ cm^{-2}\ amagat^{-2} \qquad (14)$$

$$\left(\int_0^\infty \frac{\alpha(\bar{\nu})}{N^2} d\bar{\nu} \right)_{experimental} = 8.65 \times 10^{-5}\ cm^{-2}\ amagat^{-2}$$

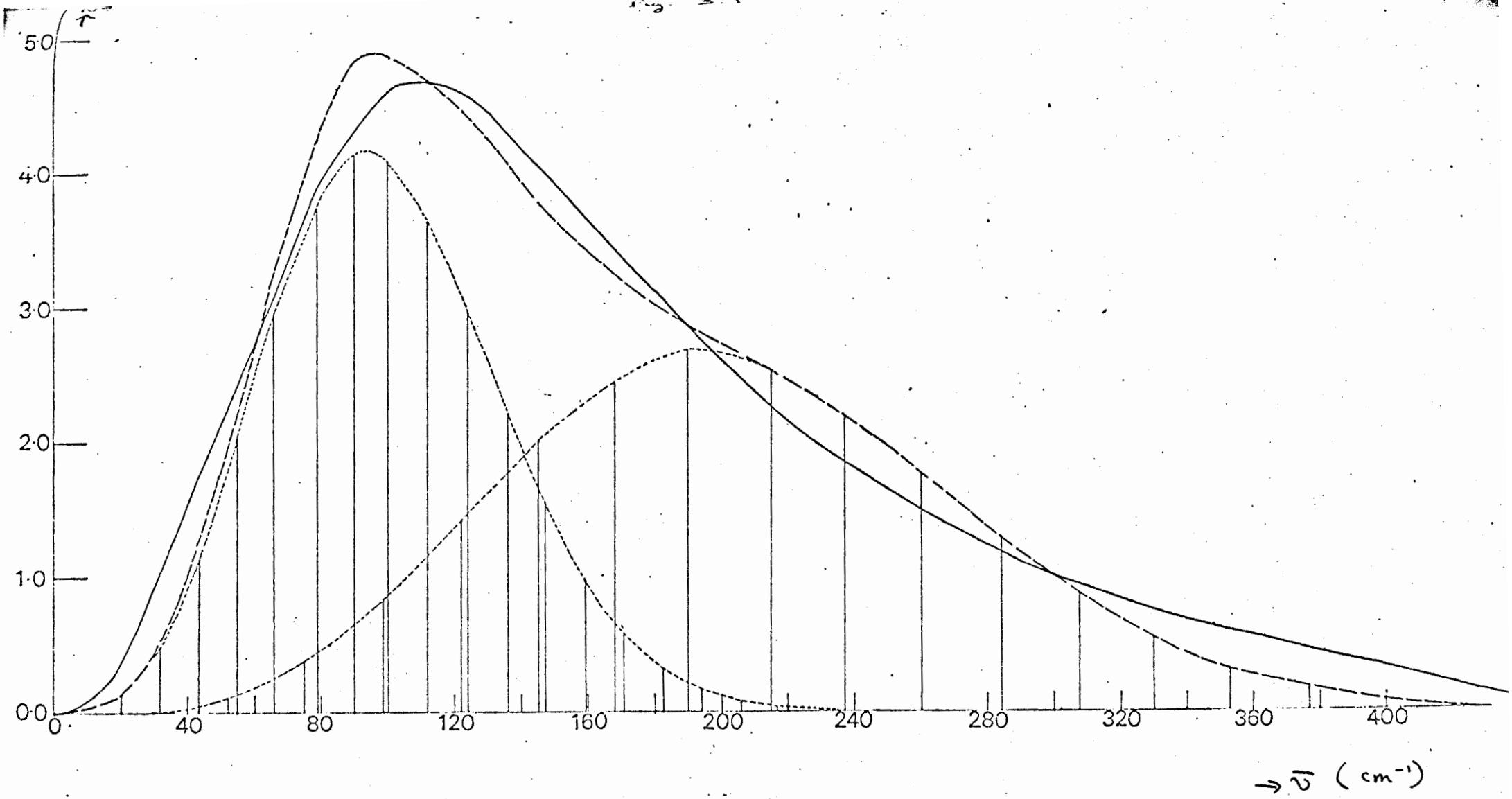
5·0
4·0
3·0
2·0
1·0
0·0
0
40
80
120
160
200
240
280
320
360
400
→ ν̃ (cm⁻¹)

Figure Caption

———— Experimental (Bosomworth and Gush, 1965).

····· Profiles of the $J \rightarrow J + 2$ (quadrupole induced) and $J \rightarrow J + 4$ (hexadecapole induced) dipole transitions.

- - - - - Overall theoretical profile.

Ordinate

$\alpha(\bar{\nu})/N^2$ (neper cm^{-1} $amagat^{-2}$)

Abscissa

$\bar{\nu}$ (cm^{-1})

Summing the L.H.S's of (13) and (14) it is found that the values of $|Q|$ and $|\Phi|$ which give the best agreement with the experimental lineshape and intensity are:

$$|Q| = 0.3 \times 10^{-26} \text{ e.s.u.} = 1.0 \times 10^{-40} \text{Cm}^2$$

$$|\Phi| = 1.1 \times 10^{-42} \text{ e.s.u.} = 3.7 \times 10^{-60} \text{Cm}^4$$

The value of $|Q|$ found compares favourably with that of -0.4×10^{-26} e.s.u. found by the induced birefringence technique (62) and $|\Phi|$ is of the correct order of magnitude, which is all that can be expected of a rough estimate such as this. Insofar as the value of $|\Phi|$ is acceptable it is justifiable to conclude that no "charge-transfer" or quasi-chemical bonding (e.g. O_4 formation) is needed to account for the pronounced difference between the absorptions of compressed O_2 and N_2 in the far infra-red.

Chapter 8.

Discussion

The general aim of this thesis has been to study the molecular interactions and motions in dense media such as those of the compressed gaseous, the liquid and the nematic phases. The complex interactions and molecular dynamics of the liquid phase are simplified a little in studies of the corresponding compressed gas, where the dynamical circumstances are changed from collision interrupted libration/diffusion to collision interrupted free rotation. The absorptions arising from the latter type of dynamics have been quantitatively treated in terms of dipoles induced in collisions involving not more than two molecules. The central part of the intermolecular potential has been approximated by a Lennard-Jones function, even though a recent review (63) has indicated that this representation is quantitatively inaccurate in all but the very simplest cases. It has been found that the uncertainties in the Lennard-Jones parameters impose the limits on subsequent values of molecular parameters (such as the quadrupole moment) deduced from the pressure induced absorptions studied in this thesis.

It must be indicated, as well, that the use of an angle dependent potential in the Colpa-Ketelaar or Frost equations would be inconsistent with the assumption that an eigenstate of the interacting pair is simply a product of eigenstates of the isolated molecules. This result is exact only if the molecules interact through a purely central potential, i.e. one independent of the Euler angles $\Theta_1, \phi_1, \chi_1, \phi_2, \Theta_2, \chi_2$. This is, then, at once a major restriction on the theory, even in the gas phase, for highly anisotropic molecules such as cyanogen, where the quadrupole-quadrupole interaction is important

and angle dependent. The further use of this theory in the liquid phase is justifiable only on the basis that some kind of approximation is better than none.

The fact that in cyanogen liquid, for example, the computed quadrupole moment is presumably of the correct order of magnitude is all that can be expected of the theory. This gives some small indication that expansion of the electrostatic molecular field in terms of point multipoles is at least valid as a quantitative starting point for investigations of non-dipolar liquids. A reasonable conclusion that can be drawn from the work on cyanogen is that the molecule has a very large quadrupole moment, possibly the largest yet encountered. The numerical value needed to explain the gas phase absorptions with the Colpa-Ketelaar theory is much reduced in the liquid phase, an observation which may indicate that the interactions of more than two molecules in the latter phase lead to a smaller nett dipole induced in any one molecule. In retrospect, therefore, it is not surprising that the $J \rightarrow J + 2$ transitions peak at a lower frequency than the experimental band; but rather how well this simple model suffices. A possible improvement would be the calculation of the hexadecapole-induced dipole ($J \rightarrow J + 4$) line spectrum, but this would still be working in the shadow of a badly known intermolecular potential - a storm thatch on clay walls.

These shortcomings apply also to the study of propyne, but there, what is apparent is the considerable shift in $\bar{\nu}_{max}$ from 18 cm^{-1} to 78 cm^{-1} on going from dilute gas to liquid. (Unfortunately, intermediate pressure data are difficult to come by without possible decomposition by overheating). The qualitative explanation of this shift is based on the transition from collision interrupted rotation

to libration-diffusion, there being quantitative theories for both processes which are fairly adequate. However, there is at present no satisfactory description of the effect of induced dipoles on the far infra-red absorptions of either dipolar or non-dipolar liquids. This is indicated by the divergence between the prediction of A/N by the Brot-Larkin or Wyllie-Larkin models (which agree with Gordon's estimate of the integrated absorption intensity per molecule arising from libration/relaxation of the permanent dipole) and the observed A/N, which in propyne liquid is much greater. This excess over the Gordon estimate has been known since the first results of Pardoe. The only way at present of treating these induced dipoles is via the multipole expansion used in Colpa and Ketelaar's theory, i.e. by treating the dynamics as collision interrupted free rotation when they are transparently not so.

This excess is probably very large in MBBA, allowing for the uncertainties in the estimated moments of inertia, but this is only to be expected (in retrospect), the motion of the molecule being anything but free rotation or libration of merely the permanent dipole alone. Probably, quite a large dipole is induced in a central molecule by the fluctuating fields of its nearest neighbours in the quite closely packed nematic phase. The sharp peak observed at the relatively high frequency of 130 cm^{-1} is compatible with a model of libration/relaxation of the permanent dipole only if the motion is taken as that about the long axis of the molecule, where the moment of inertia is not impossibly large for this high frequency process. The Brot-Larkin and Wyllie-Larkin models of libration-relaxation or itinerant oscillation produce a band shape similar to the experimental with a value of the barrier height to libration (V) of about 17 kJ $mole^{-1}$.

This value was roughly matched by one calculated from a model geometry of the MBBA nematic phase (using low angle X-ray scattering data to determine the mean intermolecular separation), estimating all combinations and permutations of bond-bond attractions and atom-atom repulsions in two sets of benzene rings hexagonally arranged around two central ones which approximated the MBBA skeleton. The subsequent estimates of V varied from 9 kJ $mole^{-1}$ to 260 kJ $mole^{-1}$, the latter being unrealistically high because the surrounding rings were held rigidly parallel as the centre one was rotated from one energy well to the next. In reality, the rings would be in a state of thermal flux (with translational freedom also), a crude approximation to which brought V down to about 9 kJ $mole^{-1}$. The hydrogen-hydrogen repulsion interaction was found to be predominant in the relevant part of the intermolecular potential.

The application of the Brot-Larkin and Wyllie-Larkin models to the flexible, substituted ethanes was an attempt to study the effect of decreasing molecular symmetry on the predicted barrier heights to libration. The exercise necessarily meant a drop in theoretical validity, since the models were originally adopted for work with the pseudo-spherical molecules whose geometry with respect to each other in a rotator phase, for instance, is well-known. There is also a large uncertainty in the effective mean moments of inertia, and this, together with the neglect of induced dipole absorption common to every application of models conforming to Gordon's equation, makes the final values of V a poorer approximation than usual. Nevertheless, they seem to be significantly higher than those typical of ''rotator-phase molecules'', which may indicate that these models are at least qualitatively adequate in describing the intuitive expectation of

increasing barrier heights to libration with increasing molecular asymmetry.

Future studies of the compressed gas-liquid kind may perhaps be most fruitful with molecules of roughly spherical geometry to which a purely central potential is a fairer approximation. (Preferably, the critical properties should be such that the gas can be compressed to liquid-like densities without danger of decomposition due to over-heating). Pseudo-spherical molecules may be expected to behave in the liquid just above the critical point as more or less collision interrupted almost-free rotors, and thereafter as progressively hindered rotors during the approach to the dense liquid state. The Frost equations could be applied (somewhat less rigorously) to non-dipolar symmetric tops of lower symmetry, such as cyclopropane or even cyclobutane.

A theory of induced dipolar absorption arising from libration/rotation/diffusion of non-dipolar molecules is needed, possibly using a tensorial correlation function as the starting point. An expansion of the molecular field in terms of charge distribution instead of point multipoles would be an improvement on the existing methods, especially for the more anisotropic cases. However, the incorporation of such a field representation into equations such as those of Frost might prove to be a complex operation.

Comparison of techniques such as ^{13}C, ^{17}O, ^{15}N, ^{1}H Fourier transform N.M.R. relaxation, slow neutron scattering, laser light scattering, Raman, and dielectric data with the far infra-red data might be instrumental in producing a more balanced overall picture of molecular dynamics in liquids, nematics, and rotator phase solids.

Far infra-red studies of liquid crystalline compounds, complemented by corresponding dilution, orienting field, and temperature studies are capable of yielding quite significant information on the local structure of these phases. These studies would be fruitful in conjunction with dielectric, high-field, and Kerr effect studies embracing the scale outside the nearest neighbouring region with which the far infra-red is associated. However, there is a need for a definitive theory of swarm formation, leading eventually to a quantitative explanation of the extended cooperative process inherent in, for instance, the sharp isotropic-nematic transition point, a phenomenon as typical of the compound as the usual phase changes.

REFERENCES

Chapter 1

1. M.F. Crawford, H.L. Welsh and J.L. Locke,
   Phys. Rev., 1949, 75, 1607.

2. J.A.A. Ketelaar, J.P. Colpa, and F.N. Hooge,
   J. Chem. Phys., 1955, 23, 413.

3. J.P. Colpa and J.A. Ketelaar,
   Mol. Phys., 1958, 1, 14.

4. Z.J. Kiss, H.P. Gush and H.L. Welsh,
   Can. J. Phys., 1959, 37, 362.

5. Z. J. Kiss and H.L. Welsh,
   Phys. Rev. Lett., 1959, 2, 166.

6. Z.J. Kiss and H.L. Welsh,
   Can. J. Phys., 1959, 37, 1249.

7. D.R. Bosomworth and H.P. Gush,
   Can. J. Phys., 1965, 43, 751.

8. W. Ho, G. Birnbaum and A. Rosenberg,
   J. Chem. Phys., 1971, 55(3), 1028;

   G. Birnbaum, W. Ho and A. Rosenberg,
   J. Chem. Phys., 1971, 55(3), 1039.

9. G. Birnbaum, A.A. Maryott and P.F. Wacker,
   J. Chem. Phys., 1954, 22, 1782.

10. S. Kielich,
    "Dielectric and Related Molecular Processes", Chem. Soc.,
    Specialist Periodical Report, 1972, 1, 230.

11. T.K. Bose and R.H. Cole,
    J. Chem. Phys., 1970, 52, 140.

12. A. Rosenberg and G. Birnbaum,
    J. Chem. Phys., 1970, 52, 683.

13. M. Evans,
    J.C.S. Faraday II, 1972, 69, 763.

14. J.P. Colpa and J.A.A. Ketelaar,
    Mol. Phys., 1958, 1, 343.

15. A.I. Baise,
    J.C.S. Faraday II, 1972, 68, 1904.

16. R.G. Gordon,
J. Chem. Phys., 1963, 38, 1724.

17. S.R. Polo and M.K. Wilson,
J. Chem. Phys., 1955, 23, 2376.

18. M.W. Evans,
Spectrochim. Acta, 1974, 30A, 79.

19. P. Debye,
"Polar Molecules", Chemical Catalog Co., 1929.

20. C.H. Cartwright and J. Errera,
Proc. Roy. Soc., A, 1936, 154, 138.

21. J. Ph. Poley,
J. Appl. Sci. B, 1955, 4, 337.

22. Y. Rocard,
J. Phys. Rad., 1933, 4, 247.

23. J. G. Powles,
Trans. Faraday Soc., 1948, 44, 802.

24. M. Davies, G.W.F. Pardoe, J.E. Chamberlain and H.A. Gebbie,
Trans. Faraday Soc., 1968, 64, 847.

25. G.W.F. Pardoe,
Trans. Faraday Soc., 1970, 66, 2699.

26. R. Haffmans and I.W. Larkin,
J.C.S. Faraday II, 1972, 68, 1729.

27. I.W. Larkin,
J.C.S. Faraday II, 1973, 69, 1278.

28. B. Lassier and C. Brot,
Chem. Phys. Lett., 1968, 1, 581.

29. B. Lassier and C. Brot,
Disc. Faraday Soc., 1969, 48, 39.

30. C. Brot,
J. de Phys., 1967, 28, 789.

31. M. Evans, M. Davies and I. Larkin,
J.C.S. Faraday II, 1973, 69, 1011.

32. G.W.F. Pardoe,
Thesis (Univ. of Wales, 1969).

33. N.E. Hill,
Proc. Phys. Soc., 1963, 82, 723.

34. G. Wyllie,
J. Phys. C, 1971, 4, 564.

35. M. Moisan,
Thesis (Univ. of Rennes, 1969).

36. I. Larkin and M. Evans,
J.C.S. Faraday II, 1974, 70, 477.

37. A.I.M. Rae and R. Mason,
Proc. Roy. Soc. A, 1968, 304, 487.

Chapter 2

38. H.A. Gebbie and R.Q. Twiss,
Rep. Prog. Phys., 1966, 29, 729.

39. G.J. Davies,
Thesis (Univ. of Wales, 1971).

40. W.J. Hurley,
J. Chem. Ed., 1966, 43, 236.

41. R. Haswell,
Sir Howard Grubb-Parsons and Co., publication.

42. J. Chamberlain,
Infra-red Phys., 1971, 11, 25.

43. K.D. Moller and W.G. Rothschild,
"Far Infra-red Spectroscopy", Wiley-Interscience,
New York, 1971, Chapt. 4, p.131.

44. J.W. Cooley, P.A.W. Lewis and P.D. Welch,
I.E.E.E. Trans. Audio and Electroacoustics, 1967,
AU - 15, 79.

45. A.I. Baise,
Thesis (Univ. of Wales, 1971).

46. E.K. Plyler, D.J.C. Yates and H.A. Gebbie,
J. Opt. Soc. Amer., 1962, 52, 859.

47. M.J.E. Golay,
Rev. Sci. Instr.,1947, 18, 357.

48. M.J.E. Golay,
Rev. Sci. Instr., 1949, 20, 816.

49. O.H. Hougen, K.M. Watson and R.A. Ragatz,
"Chemical Process Principles Charts", Wiley, N. York, 1954.

50. R.P. Cook and P.L. Robinson,
J. Chem. Soc., 1935, II, 1001.

51. J. Chamberlain,
Infra-red Phys., 1971, 12, 145.

52. J.O. Hirschfelder, C.F. Curtiss and R.B. Bird, ''Molecular Theory of Gases and Liquids'', Chapt. 5, p.362, J. Wiley, New York, 1954.

53. ''Handbook of Chemistry and Physics'', (Ed. R.C. Weast), The Chemical Rubber Co., 1972, 52, D-153.

54. A.V. Grosse and C.B. Linn, J. Am. Chem. Soc., 1939, 61, 752.

55. F.R. Morehouse and O. Maass, Can. J. Res., 1934, 11, 637.

56. P. Maurel and A.H. Price, J.C.S. Faraday II, 1973, 69, 1486.

57. V.K. Agarwal and A.H.Price, J.C.S. Faraday II, 1974, 70, 188.

Chapter 3.

58. B.S. Frost, J.C.S. Faraday II, 1973, 69, 1142.

59. M. Abramowitz and J.A. Stegun, 'Handbook of Mathematical Functions', Dover Publications Inc., New York, 1965, p.1006.

60. A.D. Buckingham and J. A. Pople, Trans. Faraday Soc., 1955, 51, 1173.

61 H.A. Stuart, 'Molekulstraktur' (Springer, Berlin, 1967) Chapt. 8, p.416.

62. A.D. Buckingham, R.L. Disch and D.A. Dunmur, J. Amer. Chem. Soc., 1968, 90, 3104.

Discussion

63. G.C. Maitland and E.B. Smith, Chem. Soc. Rev., 1973, 2(2), 181.